JGR Solid Earth

RESEARCH ARTICLE
10.1029/2020JB019570

Laramide Orogenesis Driven by Late Cretaceous Weakening of the North American Lithosphere

Joel E. Saylor[1], Kurt W. Rudolph[2], Kurt E. Sundell[3], and Jolante van Wijk[4]

[1]Department of Earth, Ocean and Atmospheric Sciences, University of British Columbia, Vancouver, British Columbia, Canada, [2]Department of Earth and Atmospheric Sciences, University of Houston, Houston, TX, USA, [3]Department of Geosciences, University of Arizona, Tucson, AZ, USA, [4]Department of Earth and Environmental Science, New Mexico Institute of Mining and Technology, Socorro, NM, USA

Abstract This paper investigates the causes of the Late Cretaceous transition from "Sevier" to "Laramide" orogenesis and the spatial and temporal evolution of effective elastic thickness (EET) of the North American lithosphere. We use a Monte Carlo flexural model applied to 34 stratigraphic profiles in the Laramide province and five profiles from the Western Canadian Basin to estimate model parameters which produce flexural profiles that match observed sedimentary thicknesses. Sediment thicknesses come from basins from New Mexico to Canada of Cenomanian–Eocene age that are related to both Sevier and Laramide crustal loads. Flexural models reveal an east-to-west spatial decrease in EET in all time intervals analyzed. This spatial decrease in EET may have been associated with either bending stresses associated with the Sevier thrust belt, or increased proximity to attenuated continental crust at the paleocontinental margin. In the Laramide province (i.e., south of ~48°N) there was a coeval, regional decrease in EET between the Cenomanian–Santonian (~98–84 Ma) and the Campanian–Maastrichtian (~77–66 Ma), followed by a minor decrease between the Maastrichtian and Paleogene. However, there was no decrease in EET in the Western Canada Basin (north of ~48°N), which is consistent with a lack of Laramide-style deformation or flat subduction. We conclude that the regional lithospheric weakening in the late Santonian–Campanian is best explained by hydration of the North American lithosphere thinned by bulldozing by a shallowly subducting Farallon plate. The weakening of the lithosphere facilitated Laramide contractional deformation by focusing end-loading stresses associated with flat subduction. Laramide deformation in turn may have further reduced EET by weakening the upper crust. Finally, estimates of Campanian–Maastrichtian and Paleogene EET are comparable to current estimates indicating that the modern distribution of lithospheric strength was achieved by the Campanian in response to flat subduction.

Plain Language Summary The western United States and Canada share an organized mountain belt which runs their length. However, in the United States there is also a series of isolated mountain ranges to the east of that organized belt. This difference is often attributed to the shallow descent of an oceanic tectonic plate beneath the western United States between about 90 and 45 million years ago (Ma), and steeper descent beneath Canada. However, it is unclear why this would produce the differences observed at the surface. We examine this question by reconstructing the strength of the North American tectonic plate from 90–45 Ma, by modeling its rigidity (resistance to bending). In the model we apply random loads and stiffnesses to observe how the modeled plate bends to form sedimentary basins and accommodate sediment accumulation. We then compare the results of this Monte Carlo model to observed sediment thicknesses in real basins to determine which set of parameters match observations. Our results are most consistent with weakening of the USA portion of the North American plate by incorporation of fluids from the shallowly descending oceanic plate. This weakening focused deformation in the region directly above the shallow plate leading to spatially limited deformation.

Key Points:
- Monte Carlo flexural modeling shows temporal and spatial variations in effective elastic thickness of the North American lithosphere from Late Cretaceous–Eocene
- Santonian–Campanian lithospheric weakening is best explained by introduction of fluids to the North American lithosphere during flat subduction
- Lithospheric weakening enhanced Laramide deformation by focusing end-loading stresses associated with flat subduction

Supporting Information:
- Supporting Information S1
- Data Set S1
- Data Set S2
- Data Set S3
- Data Set S4
- Data Set S5

Correspondence to:
J. E. Saylor,
jsaylor@eoas.ubc.ca

Citation:
Saylor, J. E., Rudolph, K. W., Sundell, K. E., & van Wijk, J. (2020). Laramide orogenesis driven by Late Cretaceous weakening of the North American lithosphere. *Journal of Geophysical Research: Solid Earth*, *125*, e2020JB019570. https://doi.org/10.1029/2020JB019570

Received 11 FEB 2020
Accepted 28 JUL 2020
Accepted article online 5 AUG 2020

1. Introduction

The strength of continental lithosphere plays a fundamental role in determining the nature of lithosphere deformation and basin formation. In the North American Cordillera, the strength of the lithosphere has been correlated with spatial variations in effective elastic thickness (EET) (Bechtel et al., 1990; Bills &

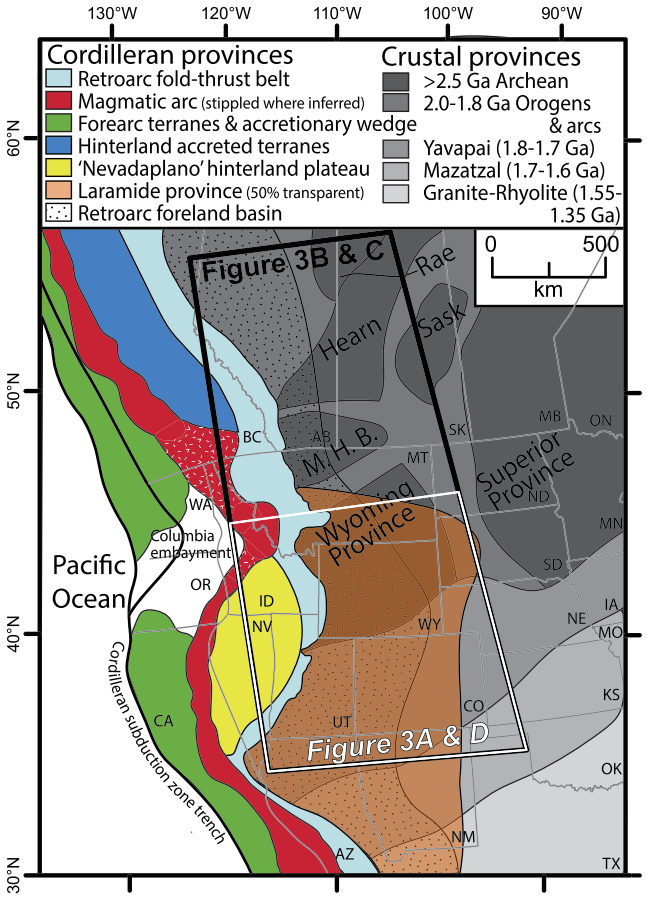

Figure 1. Map of North America in the Late Cretaceous showing the major tectonic elements and the location of Figure 3. Abbreviations for states and provinces: AB, Alberta; AZ, Arizona; BC, British Columbia; CA, California; CO, Colorado; IA, Iowa; ID, Idaho; KS, Kansas; MB, Manitoba; MN, Minnesota; MO, Missouri; MT, Montana; NE, Nebraska; ND, North Dakota; NM, New Mexico; NT, Northwest Territories; NV, Nevada; OK, Oklahoma; ON, Ontario; OR, Oregon; SD, South Dakota; SK, Saskatchewan; TX, Texas; UT, Utah; WA, Washington; WY, Wyoming. Abbreviations for crustal provinces: M.H.B., Medicine Hat block. Cenozoic extension in the western USA is palinspastically restored. No palinspastic restoration was applied to Canada. Modified from DeCelles (2004), Whitmeyer and Karlstrom (2007), Dickinson (2013), Nelson et al. (2013), Hildebrand (2014), Yonkee and Weil (2015), and Yonkee et al. (2019).

May, 1987; Fulton & Walcott, 1975; Karner & Watts, 1983; Lowry & Smith, 1994; Quinlan & Beaumont, 1984; Sheffels & McNutt, 1986; Tesauro et al., 2015; Walcott, 1970). The region affected by Laramide deformation (i.e., the "Laramide province," south of ~48°N), which occupies an area up to 700 km east of the Sevier thrust front in Wyoming and western Nebraska (Figure 1) (DeCelles, 2004; Dickinson et al., 1988; Dickinson & Snyder, 1978; Lawton, 2008; Yonkee & Weil, 2015), is characterized today by anomalously low elastic plate thickness (EET < 30 km) and considered weak (Hyndman et al., 2009; Tesauro et al., 2015). Here, "thick-skinned" Laramide deformation involved basement-cored uplifts and widely spaced thrust faults that extend to midcrustal depths (e.g., Wind River Uplift, Stevens et al., 2016). North of the Laramide province (north of ~48°N), the EET exceeds 100 km within 50 km of the Sevier thrust front and is described as strong lithosphere (Hyndman et al., 2009; Tesauro et al., 2015). "Thin-skinned" Sevier deformation in this part of the Cordillera involved internally deformed, closely spaced thrust sheets composed primarily of upper crustal sedimentary or metasedimentary rocks.

EET is not itself a physical thickness of the lithosphere or any mechanical layer in the lithosphere. Rather, it is the thickness of an idealized plate used to model the elastic response of the lithosphere and represents the integrated brittle, elastic, and ductile strength of the lithosphere (after Burov & Diament, 1996; Watts & Burov, 2003). Hence, weakening of any of the rheological layers of the lithosphere or decoupling of the upper crust and mantle will result in a decrease in EET (Burov & Diament, 1996). Basins formed by flexure of weak (i.e., low EET) lithosphere are short-wavelength, large-amplitude structures. In contrast, lithospheric mantle that is strong and/or lithosphere that is fully coupled results in high EET, and deformation produces long-wavelength, small-amplitude flexural basins. The geometry of sedimentary basins thus provides information about the strength of the associated plate.

Although the current EET of the western North American lithosphere is well known, *when* it attained this EET distribution is only documented in the Wyoming segment of the Laramide province. There, the current EET was established by the Paleocene (Gao et al., 2016). We extend the analysis of Gao et al. (2016) to a region that spans from New Mexico to Canada to document temporal and spatial changes in effective elastic thickness and orogenic load of the North American Cordillera. Results of our analysis are used to discriminate between existing models for EET modification during the Laramide (Figure 2).

Models that have been proposed for lithospheric weakening and EET reduction associated with Laramide deformation can be combined into four groups (Figure 2). These groups of models make unique predictions about the timing and extent of rheological modification of the North American plate. Hence, the temporal and spatial distribution of lithospheric strength and orogenic loading is a key discriminant between the models. In Group 1, heating of the North American plate during the inboard sweep of volcanism that accompanied flattening and advance of the Farallon slab weakened the lithosphere (Figure 2) (cf. Coney & Reynolds, 1977; Constenius et al., 2003; Copeland et al., 2017; Hyndman et al., 2009). This model predicts that upper plate weakening was synchronous with Farallon slab flattening and advanced toward the continent interior at the same rate as the inboard sweep of magmatism. In Group 2, weakening of the North American plate accompanied removal of the flat Farallon slab (Figure 2) (Humphreys, 2009). Removal of the flat slab reopened the asthenospheric wedge, resulting in magmatism, heating, and potentially weakening of the upper plate. In this model weakening of the North American plate would have occurred in the Cenozoic, accompanying or following flat slab rollback. In Group 3, the advancing Farallon flat slab

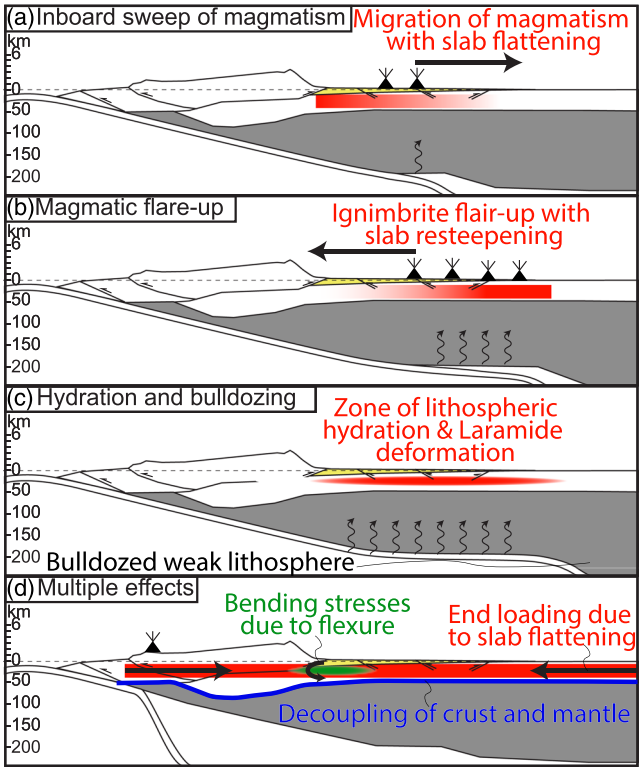

Figure 2. Schematic presentation of four groups (a–d) of models proposed for weakening of western North American lithosphere (see text for references). Colored zones correlate to the regions impacted by the proposed mechanism. Cartoons are intended to depict the geographic extent, relative impact, and timing of weakening and do not imply that weakening occurs at the depth indicated.

thinned the North American lithosphere via ablation or "bulldozing" of mantle lithosphere material (Axen et al., 2018). This, accompanied by hydration of the North American lithosphere during flat subduction, would weaken the lithosphere of the overriding plate during flat subduction (Figure 2c) (Humphreys et al., 2003). Group 3 predicts that initial weakening occurred primarily as the lower plate was heated and lost fluids while in contact with the upper plate. Dehydration of the lower plate, and therefore weakening of the upper plate, would be delayed relative to the initiation of flat subduction by the time needed to heat serpentinized oceanic mantle to temperatures of 600–700°C or subduct it to depths > ~200 km. This provides sufficient time to transport hydrous mineral phases >1,200 km inboard from the trench (Currie & Beaumont, 2011; Schmidt & Poli, 2003; Sommer & Gauert, 2011). In Group 4, several processes played a role in EET reduction. Gao et al. (2016) suggested that a southwestward decrease in EET in the Paleogene Wyoming province was due to a combination of (a) a decrease in the radius of curvature of the North American plate due to flexure by the Sevier topographic load (Burov & Diament, 1995), (b) decoupling of the crust and mantle (Burov & Diament, 1996), and (c) horizontal, contractional stresses transmitted from the trench across the North American plate (also known as, end-loading) due to shallow subduction (Axen et al., 2018; Burov & Diament, 1995) (Figure 2d). Group 4 predicts plate-wide upper plate weakening occurred prior to and continued during flat subduction.

In this study, we track the spatial and temporal evolution of EET and orogenic loads in western North America via Monte Carlo forward flexural modeling of stratigraphic profiles. We consider 39 stratigraphic profiles from the San Juan Basin of New Mexico to the Canadian foreland basin of southern Alberta (Figure 1) to constrain the spatial evolution of EET. Profiles span the Cenomanian–Eocene (~95–34 Ma), allowing us to track temporal changes in EET. For each stratigraphic profile we calculate the EET and orogenic load that produce a flexural profile which matches the stratigraphic profile. This approach is different from existing EET estimates in North America, which are based on rheological and thermal models derived from joint inversion of gravity and seismic tomography data (Tesauro et al., 2014, 2015), and cross-spectral analysis of topography and the gravity field (Bechtel et al., 1990; McKenzie & Fairhead, 1997).

Our analysis shows that there was a spatial gradient in EET in the Cenomanian-uppermost Santonian (~98–84 Ma), with lower EET approaching the Sevier thrust front. A major initial decrease in EET between the uppermost Santonian (~84 Ma) and middle Campanian (~77 Ma) affected the lithosphere in the Laramide province (Figure 1), but did not impact the Western Canada Basin. We also find evidence for a second, minor decrease in EET between the Late Cretaceous and Paleogene (i.e., at ~ 66 Ma) in the middle of the Laramide province as suggested by Gao et al. (2016).

2. Geological Setting

Jurassic–Paleogene subduction along the western margin of Laurentia resulted in development of an Andean-style margin with a forearc, magmatic arc, retroarc fold thrust belt and foreland basin system (Figure 1) (DeCelles, 2004; Yonkee & Weil, 2015). In the western USA, subduction produced an Altiplano-style retroarc plateau in the Late Cretaceous, termed the "Nevadaplano" (Figure 1) (Bonde et al., 2015; Snell et al., 2014). Subsidence in the retroarc foreland basin (Figure 1) was driven by a combination of lithospheric flexure due to loading by thrust sheets, sediment accumulation and redistribution, and dynamic subsidence related to mantle convection (Catuneanu et al., 1997; Gurnis, 1992; Jordan, 1981; Liu & Nummedal, 2004; Mitrovica et al., 1989). Loading by thrust sheets in the Sevier belt (Figure 1), which extends from Canada to southeastern California (Armstrong, 1968; Burchfiel & Davis, 1972;

Dahlstrom, 1970; DeCelles, 2004; Price & Mountjoy, 1970; Yonkee & Weil, 2015), produced a flexural wave that migrated eastward in lockstep with the migrating fold-thrust belt (DeCelles & Giles, 1996). This resulted in an asymmetric foreland basin which was deepest adjacent to the fold-thrust belt, shallowed to the east, and paralleled the Sevier deformation front (Figure 1) (DeCelles, 2004).

Farallon plate subduction proceeded at a high angle from the Jurassic–Late Cretaceous, but shallowed beneath the present-day western United States between the Late Cretaceous and early Eocene (Coney & Reynolds, 1977; Dickinson & Snyder, 1978; Liu et al., 2010). Shallowing of the Farallon plate is supported by multiple lines of evidence, including a lull in magmatism in the arc, shallow underplating of subduction zone mélange, and exhumation of basement-cored uplifts in the former foreland basin (Coney & Reynolds, 1977; Constenius et al., 2003; Dickinson & Snyder, 1978; Lawton, 2008; Saleeby, 2003; Strickland et al., 2018). Shallowing of the subducting Farallon plate is inferred to be the result of a combination of increased trenchward motion of the North American plate, subduction of buoyant oceanic lithosphere (i.e., young or with anomalously thick crust such as the conjugate Shatsky Rise), and slab breakoff at the leading edge of the subducting plate (Engebretson et al., 1985; Liu et al., 2010; Liu & Currie, 2016; Livaccari et al., 1981; Sigloch et al., 2008; Torsvik et al., 2008; Yonkee & Weil, 2015). Geochemical evidence points to a hydrated continental mantle lithosphere below the crust of the North American plate (Lee, 2005; Lee et al., 2001; Li et al., 2008; Livaccari & Perry, 1993). This mantle hydration and associated metasomatism has been attributed to juxtaposition of oceanic lithosphere beneath North American lithosphere during flat subduction (Humphreys et al., 2003).

"Laramide" compressional deformation of the North American plate along moderate-angle (i.e., 25–40°) crustal ramps may have begun as early as 90 Ma in the northern Green River Basin (Wyoming) and southwestern Montana (Carrapa et al., 2019; Schwartz & DeCelles, 1988; Shuster & Steidtmann, 1988), but peaks in the Maastrichtian–early Eocene (Clinkscales & Lawton, 2014; DeCelles et al., 1987, 1991; Dickinson et al., 1988; Fan & Carrapa, 2014; Lawton, 2008; Peyton & Carrapa, 2013; Tindall et al., 2010). Deformation has been attributed to multiple mechanisms, including basal traction between the flat oceanic slab and the upper plate (Bird, 1988; Dickinson & Snyder, 1978), horizontal transmission of stress from the trench during flat subduction ("end-loading") (Axen et al., 2018; Livaccari & Perry, 1993), a response to dynamically driven foreland subsidence (Jones et al., 2011), and transpression due to accretion of an exotic terrane (Johnston, 2001). This deformation partitioned the Sevier foreland basin into a series of smaller basins bounded by basement-cored uplifts (e.g., Erslev et al., 1993) and reactivated some inherited lithospheric weaknesses such as the boundary between the Yavapai and Wyoming terranes (Figure 1) (e.g., Kelley, 2005; Stone, 2002). Deformation and loading of the lithosphere resulted in formation of flexural stratigraphic wedges adjacent to Laramide uplifts. These basins track the peak of Laramide deformation in the Maastrichtian, Paleocene, and Eocene, and are used in this study to calculate EET during Laramide orogenesis (Figures S1–S25 in the supporting information) (Gao et al., 2016; Jordan et al., 1988; Lynds & Lichtner, 2016).

In the Eocene–Oligocene, voluminous calc-alkaline volcanic rocks with subduction-related geochemical signatures were erupted in the Laramide province (Best et al., 2009; Coney, 1980; Coney et al., 1978). This volcanic activity is typically attributed to removal or steepening of the shallowly subducted ocean slab and impingement of hot asthenosphere on hydrated North American lower lithosphere (Armstrong & Ward, 1991; Humphreys, 1995; Humphreys et al., 2003; Livaccari & Perry, 1993) as is seen in the central Andes (DeSilva et al., 2006; Kay & Coira, 2009; Zandt et al., 2003).

3. Methods

Flexural modeling is an established method of determining EET and identifying the drivers of accommodation creation (e.g., Allen & Allen, 2005; Gao et al., 2016; Lynds & Lichtner, 2016; Lyon-Caen & Molnar, 1983; Saylor et al., 2017; Turcotte & Schubert, 1982; Wangen, 2010; Watts, 2001). We developed a two-dimensional flexural modeling approach and applied it to 39 stratigraphic profiles from flexural basins spanning southern Canada to northeastern New Mexico (Figures 3 and 4, Table S1, and Figures S1–S25 in the supporting information). Profiles were selected to cross a wedge of sediment which thickens toward a tectonic load: either the Sevier fold-thrust belt, or discrete Laramide uplifts. The modeling approach described below, including

modeling as both an infinite and broken plate (Figure 5), was applied to all 39 stratigraphic profiles. Flexural modeling inputs and outputs are included in Tables S2, S3, and S4 in the supporting information.

3.1. Modeling Approach

Flexural models were developed for 39 stratigraphic cross sections (Figure 4, locations shown in Figure 3). In each of the models, the elastic plate bends under the load of a Sevier or Laramide thrust, and the predicted geometry of the bent plate was compared with (and constrained by) the stratigraphic cross section. Prescribed parameters of the models included the stratigraphic cross sections, represented by locations and amounts of subsidence ("control points"); the number of blocks from which the load was constructed; the density of the mantle and the material that fills the accommodation produced ("infill density"); gravitational acceleration; Young's modulus; Poisson's ratio; and load geometry. The load geometry can be either rectangular or taper toward the basin (cf. Figures 5a and 5c). For the models presented here, EET was assumed to be constant over the profile distance. We also modeled several profiles with EETs that randomly linearly increased or decreased over the profile distance and found that the means of the variable constant EETs were within uncertainty. Parameters for each model are available as input files (Table S2) for the FlexMC software package (supporting information Software 1) and are summarized in Table S3.

Unknown parameters of the flexural models which were estimated using Monte Carlo simulation include load height, width, and density, and the EET of the flexed plate. The software recursively calculates between 10^4 and 10^5 model profiles; randomly varying these parameters between specified bounds in each trial. The combination of parameters that resulted in a deflected profile within a specified vertical uncertainty of the control points was used to calculate the means and standard deviations of the output parameters. Each stratigraphic cross section is represented by three to five control points. These control points were spaced as widely as possible and span the distance over which there were constraints on stratigraphic thicknesses. Stratigraphic thicknesses extrapolated over long distances or interpolated based on adjacent regions were not used as control points.

In the following paragraphs we identify four potential sources of uncertainty and describe how we address each. The first two sources of uncertainty are (1) the uncertainty introduced by the datum process described below and (2) the quality of the stratigraphic correlations and maps on which our analysis relies. Prior to flexural modeling we applied a datum correction to account for sediment accumulation above the flexural forebulge which is unassociated with lithospheric flexure (Jordan, 1981; Liu et al., 2014; Liu & Nummedal, 2004). The datum correction was applied by removing half of the thickness above the shallowest point on the flexural profile. This approach accounted for sediment accumulation unrelated to flexure and minimized flattening of the profile in cases where the forebulge was not identifiable. However, it also introduced some uncertainty into the flexural profiles. To account for the uncertainty introduced by the datum process, we assigned a vertical uncertainty of 10% of the maximum deflection prior to the datum correction to all stratigraphic-thickness control points along the profiles (Figure 5). This yielded a consistently applicable method where uncertainty was between 1σ and 2σ of the datum correction for almost all (93%) of the selected profiles. The second source of uncertainty is the quality of the stratigraphic correlations or maps underlying the profiles. This uncertainty arises from both the reliability of the interpreted surfaces and the density of the well log and outcrop control points. While this is inherently unquantifiable because it relies on qualitative assessments, comparison of maps from different sources for a few cases where this is available indicate that the isopach patterns are reasonably reliable (e.g., Maastrichtian isopach maps from northeast Green River Basin by Johnson et al. (2004) and Lynds and Lichtner (2016). Additionally, comparison of the uncertainty estimates from above (mean uncertainties of 143 ± 102 m (1σ, range of 21 to 488 m)) to the thickness of Upper Cretaceous–Paleogene stratigraphic correlation units in the Western Interior Basin (formations or parasequences within formation) suggests that the quantitative uncertainty subsumes the uncertainty in the qualitative correlations. This uncertainty is the primary source of uncertainty in the models. Its greatest impact is on Paleocene–Eocene profiles where enclosed Laramide basins facilitated the aggradation of a thick, "silled" nonmarine section.

The third potential source of uncertainty is in the horizontal distance between the load and stratigraphic control points. For profiles where stratigraphic-thickness control points were affected by postdepositional shortening, we palinspastically restored them to their predeformational location using shortening estimates from Yonkee and Weil (2015). This correction increased the wavelength of the restored flexural profile and

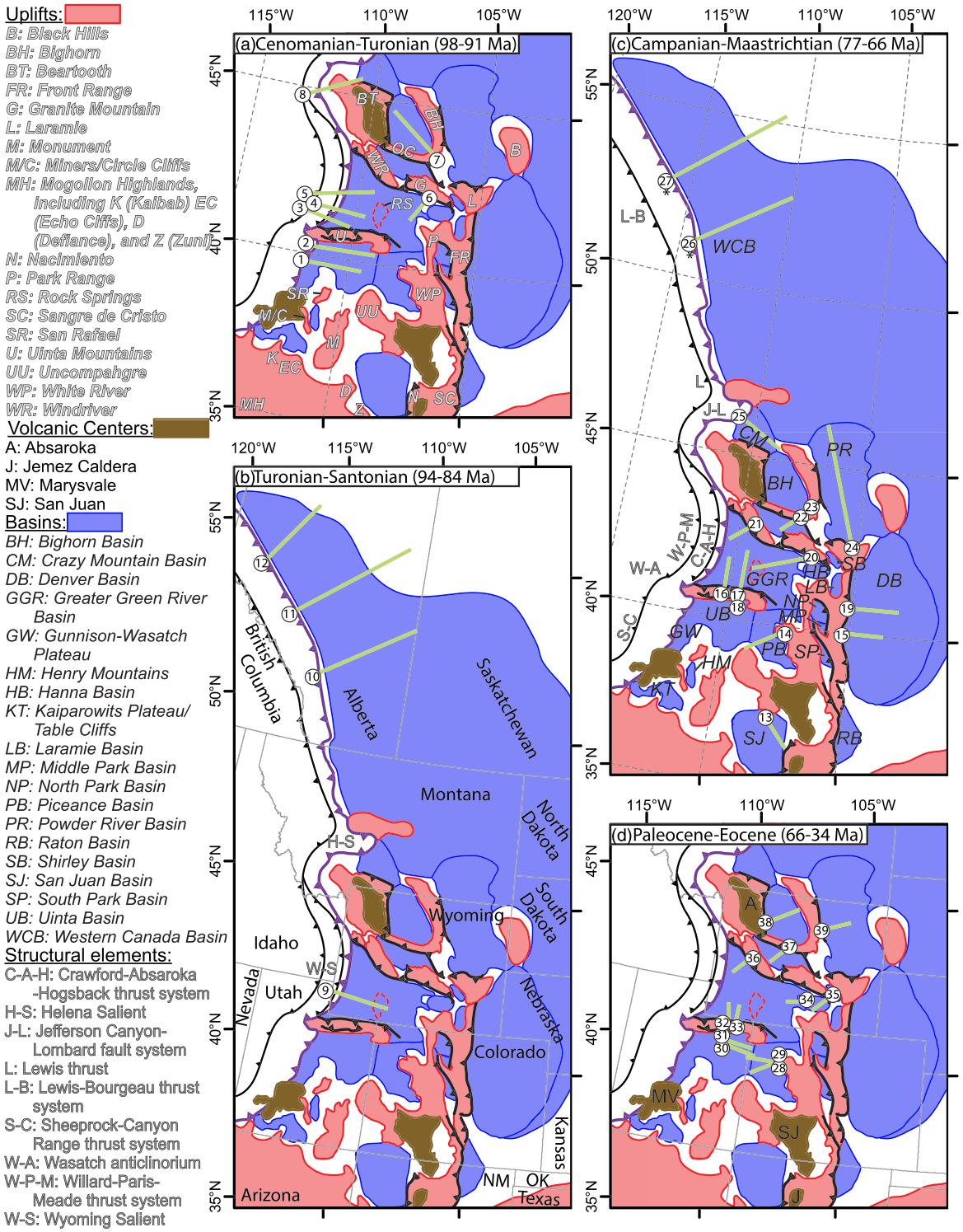

Figure 3. Schematic maps showing the location of flexural profiles relative to tectonic elements in the Late Cretaceous and early Cenozoic Sevier and Laramide orogenies. Profile numbers are placed at the location of the deepest part of the profile and correlate to stratigraphic profiles shown in Figure 4. Profile details are available in appendix materials. (a) Cenomanian–Turonian (~98–91 Ma) profiles and the location of Late Cretaceous–Cenozoic uplifts. (b) Turonian–Santonian (~94–84 Ma) flexural profiles and state or province boundaries. (c) Campanian–Maastrichtian (~77–66 Ma) flexural profiles and basin locations. Note that Profiles 26 and 27 (marked with an *) include upper Santonian strata. (d) Paleocene–Eocene (~66–64 Ma) flexural profiles and the location of Cenozoic volcanic centers. Uplifts are based on the approximate location of top Triassic exposures, and basins are based on the approximate location of base Campanian exposures. Abbreviations: OK, Oklahoma; NM, New Mexico.

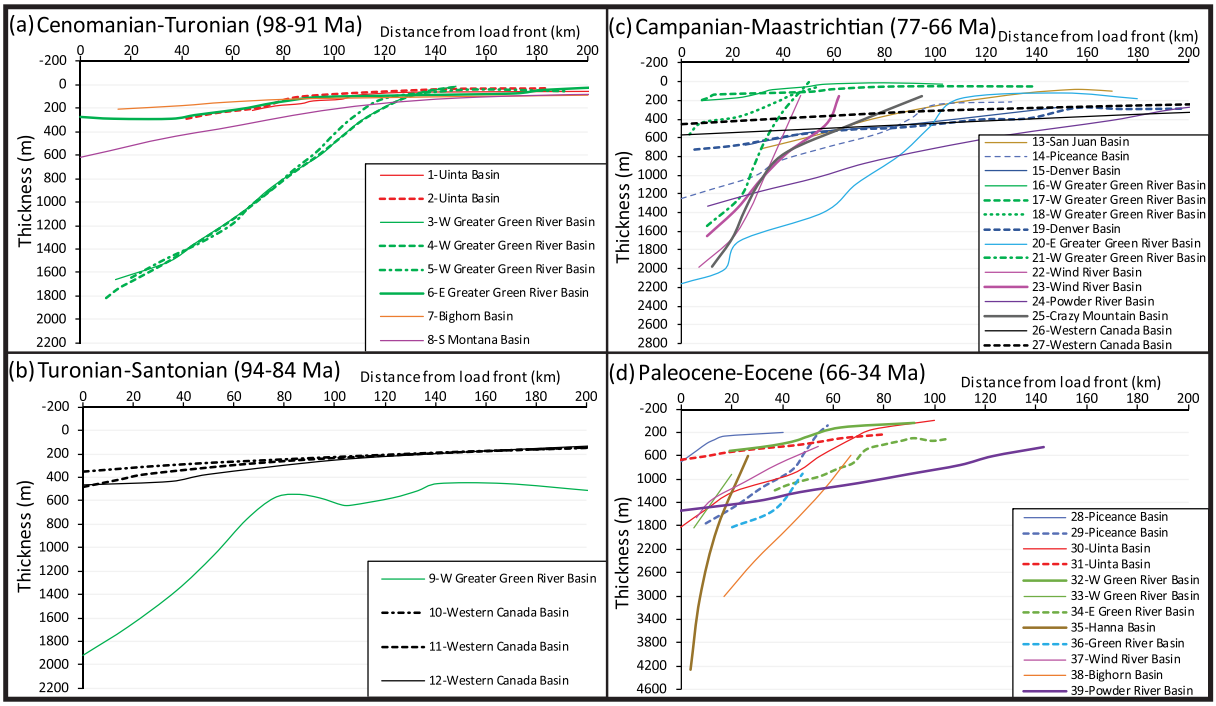

Figure 4. Flexure profiles for (a) the Cenomanian–Turonian, (b) Turonian–Santonian, (c) Campanian–Maastrichtian, and (d) Paleocenen-Eocene from basins shown in Figure 3. See supporting information Figures S1–S25 for isopach maps which these profiles are based on and Table S1 for data sources.

so resulted in greater EET over an uncorrected profile. For Laramide uplift loads, this uncertainty is generally low, because the load has not experienced any significant postdeformational translation. The reliability of the constraining information is summarized in the "quality" parameter in Table S1. We also tested the sensitivity of the model to the distance between the control points and the load by systematically moving the control points and tracking the effect on modeled EET and load height (Figure S26).

Finally, there is uncertainty introduced by projection of a three-dimensional load and basin onto a two-dimensional profile. There is a three-dimensional aspect to all loads and basins. This is particularly true for Laramide uplifts and wedges due to their relatively short strike-parallel length. The use of two-dimensional models to simulate flexural effects may tend to underestimate loads in the center of the uplift and overestimate loads on the plunging ends. We assessed the impact of this on load and EET estimates by comparing five along-strike stratigraphic profiles for the Wind River Uplift. Profiles extended southward from the Wind River Uplift parallel to Profile 21 (Figure 3c), which is the central profile.

3.2. Load Geometries

In flexural models that were related to Sevier fold-thrust belt loads, the load was pinned at the interpreted deformation front, the load width was allowed to vary between 25 and 100 km, and a taper into the basin was assumed (Figure 5). For Sevier loads we also constrained the average surface slope to be no greater than 6°, based on the maximum surface angle for noncohesive granular material with a weak basal decollement observed in critical taper sandbox experiments (Dahlen, 1990). For flexural models associated with Laramide uplifts, the load was also pinned at the deformation front, but the load width was fixed using an estimate developed from geologic maps. The load was assumed to be symmetrical (Figure 5c). For a number of the Laramide uplifts we also developed models with asymmetric load geometries; the EET results were similar, but the goodness of fit to the stratigraphic profile was less satisfactory.

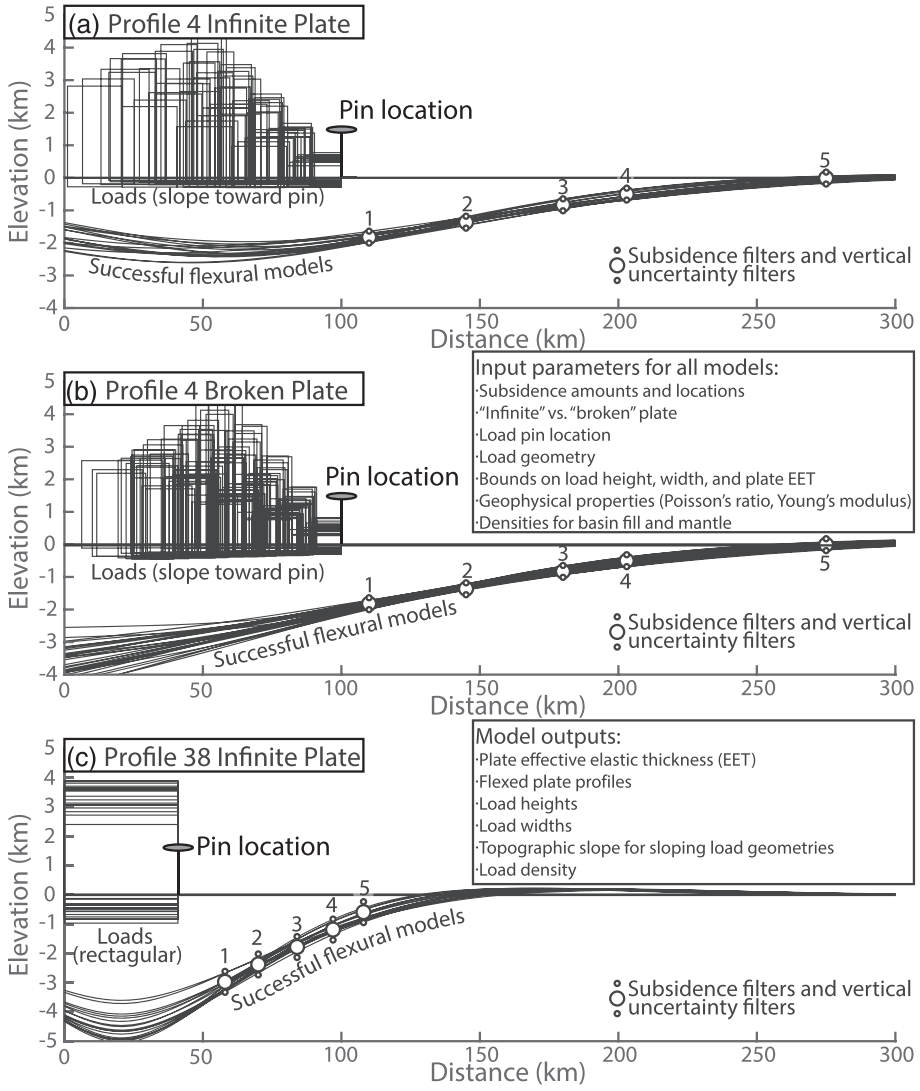

Figure 5. Example model outputs showing (a) a "Sevier load" which tapers toward the basin with a maximum surface slope of 6°. Total load width is randomly selected between 25 and 100 km. Flexure is modeled as an infinite plate and only flexural profiles that pass within the prescribed uncertainty of known subsidence locations (numbers 1–5) are accepted. (b) A "Sevier load" with flexure modeled as a broken plate. Other parameters as for (a). (c) A "Laramide load" modeled as rectangular blocks with a fixed width. Flexure is modeled as an infinite plate.

3.3. Flexural Equations and MATLAB Code

The stratigraphic profiles ("control points") were input as a primary constraint into a forward modeling MATLAB© code, "FlexMC" (Software S1, modified from Saylor et al., 2017). The algorithm uses the equations set out by Wangen (2010) to model flexed plates that are infinite in the x direction. In this parameterization, the distributed load is treated as a series of rectangular loads of height h_i and width w_i. The loading force, calculated as

$$V_i = \rho_l \, g \, h_i \, d_i, \tag{1}$$

is applied at the center of the load. In Equation 1 ρ_l is the density of the load in kg m^{-3} and g is gravitational acceleration in m s^{-2}. The deflection of the flexed plate, d, can be calculated as the sum of the deflection of N individual loads

$$d(x) = \sum_{i=1}^{i=N} \frac{V_i}{2\,\Delta\rho\,g\,\alpha}\,[\exp(-l_x)(\cos l_x + \sin l_x)] \tag{2}$$

where

$$l = \frac{|x - x_{ci}|}{\alpha} \tag{3}$$

and x is the horizontal dimension, x_{ci} is the x location of the center of the ith load block, α is the flexural parameter, and $\Delta\rho$ is the density difference between the material being displaced and the material filling the area displaced by the flexed plate. In order to model a plate that is semi-infinite in the x direction (i.e., broken at $x = 0$) we use the following equations from Hetenyi (1979, chapter 2):

$$A = \exp\left(\frac{-x}{\alpha}\right)\left(\cos\frac{x}{\alpha} + \sin\frac{x}{\alpha}\right) \tag{4}$$

$$B = \exp\left(\frac{-x}{\alpha}\right)\left(\sin\frac{x}{\alpha}\right) \tag{5}$$

$$C = \exp\left(\frac{-x}{\alpha}\right)\left(\cos\frac{x}{\alpha} - \sin\frac{x}{\alpha}\right) \tag{6}$$

$$D = \exp\left(\frac{-x}{\alpha}\right)\left(\cos\frac{x}{\alpha}\right) \tag{7}$$

$$Y = (C_{x_{ci}} + 2\,D_{x_{ci}})A_x - 2\,(C_{x_{ci}} + D_{x_{ci}})B_x + [\exp(-l_x)(\cos l_x + \sin l_x)] \tag{8}$$

$$d = \sum_{i=1}^{i=N} \frac{-Y\,V_i}{2\,\Delta\rho\,g\,\alpha} \tag{9}$$

In Equations 4–7 x terms are replaced by either the x dimension or the x location of the center of the ith load (x_{ci}) as indicated by the subscripted terms in Equation 7. All models assume that the load and flexed beam are infinite in the z direction (i.e., into the plane of the page).

4. Characteristics of the Flexural Profiles

The 34 flexural profiles from the United States western interior display considerable variability in the amplitude and wavelength of flexure, whereas the five profiles of the Western Canada Basin all have long (>200 km) wavelength and small (<600 m) amplitude (Figure 4 and Table S3). For the upper Cenomanian–Turonian (~98–91 Ma) interval, five Sevier-related foredeep profiles have been constructed from central Utah to southern Wyoming (Profiles 1, 2, 3, 4, and 5). The amplitude of the three northern profiles (W. Greater Green River Basin, southern Montana Basin; 1,600–2,000 m) is an order of magnitude greater than that of the two southern profiles (Uinta Basin, Bighorn Basin; 200–300 m), although the basin widths are similar (150–200 km). Profile 6 from the eastern Greater Green River Basin, which may be the result of early Laramide deformation, has a maximum deflection of ~300 m and a basin width of 150–200 km. The upper Cenomanian–Turonian (~98–91 Ma) profile from southern Montana (8), and Turonian–Santonian (~94–84 Ma) Western Canada Basin profiles (10, 11, and 12) have long wavelengths (>250 km). The single, low-confidence profile that we have from the Green River Basin during the Coniacian-Santonian interval (Profile 9, ~91–84 Ma) displays a shorter wavelength (125 km) than any older United States profiles.

The 27 profiles for the Campanian through Eocene wedges are typically shorter wavelength, but higher amplitude (50–100 km, 200 to >4,000 m, respectively). However, both parameters are extremely variable. Nearly all profiles are associated with intraforeland Laramide uplifts; only the Crazy Mountain Basin (Profile 25) has been identified as a possible Sevier-related foredeep.

Flexural forebulges are difficult to identify in our profiles because the upward deflection is small; generally 4–7% of the downward deflection of the foredeep (DeCelles, 2012). As a result, complicated 3-D effects, bathymetric/topographic relief, or minor errors in stratigraphic thickness estimates can mask the forebulge. Nevertheless, we identify five forebulges, providing additional confirmation of a flexural subsidence

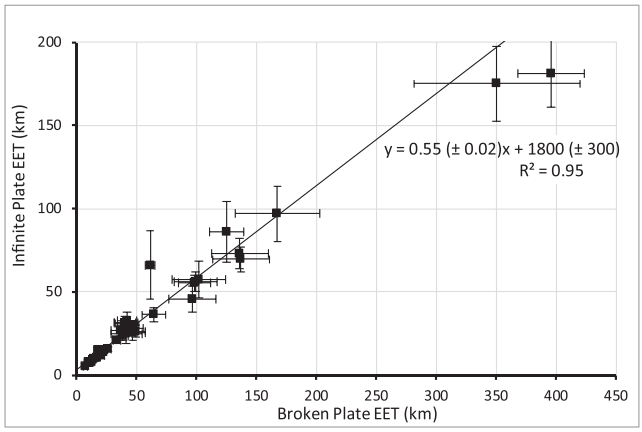

Figure 6. Cross-plot of effective elastic thickness calculated using an infinite versus a broken-plate flexural model. Effective elastic thicknesses modeled assuming a broken plate are roughly double those calculated using an infinite plate model and yield unreasonably high effective elastic thicknesses.

mechanism for both the Sevier foreland and Laramide basins. First, a persistent thin of the Cenomanian–Turonian isopach occurs about 150–250 km east of the Sevier load (Figure S1). This can be recognized for over 1,000 km, from south to north (DeCelles, 2004; DeCelles & Giles, 1996; Robinson-Roberts & Kirschbaum, 1995). A similar thin, aligning with the subsequent Moxa Arch, occurs in the Coniacian–Santonian interval in the Green River Basin (Figure S6). Positive features are indicated by stratigraphic thins in at least three Maastrichtian examples. The Douglas Creek Arch, separating the Uinta and Piceance Basin, lies about 80 km west of the White River Uplift and its associated flexural wedge (Figure S14). The Moxa Arch in the western Green River Basin is a Laramide-style uplift that displays middle Campanian growth, including erosion of up to 1 km of older sedimentary section (Devlin et al., 1993; Roehler, 1965; Rudolph et al., 2015). Over most of its ~200 km extent, the Moxa Arch has little to no post-Campanian deformation. However, at its northern end, the Moxa Arch is rejuvenated and shows significant Maastrichtian and Paleocene structural relief and thinning (Figure S12). This has previously been interpreted as related to the interaction of the encroaching Sevier thrust system (Becker et al., 2010; Becker & Lynds, 2012; Kraig et al., 1988). Alternatively (or additionally), the rejuvenation of the northern Moxa Arch may be a forebulge related to the Wind River Mountains, 70 km to the northeast. The fifth example is a subtle Maastrichtian thin within the Powder River Basin, ~200 km north of the Hartville-Laramie Mountains load (Figure S13). These forebulges confirm that load-induced flexure of the lithosphere is a widespread and important element of sedimentary accommodation and basin formation throughout the study interval.

5. Modeling Results

The broken-plate flexural models produce EETs that are approximately twice those from infinite plate models (Figure 6). EETs estimated using a broken plate model are poorly correlated with modern EETs regardless of the time window considered. For example, 25% (10 of 39) of the broken plate models yield EETs >70 km, and two yield EETs as high as 300–400 km (Figure 6). The present-day EET of the North American Cordillera and Laramide province is generally less than 60 km, with maximum modern EETs in North America ~200 km (Figure 8 of Tesauro et al., 2015). In contrast, Campanian–Eocene EETs based on an infinite plate model are well correlated to modern EETs. The broken plate model assumes that all of the orogenic load is applied to one limb of the broken plate. We conclude that the implausibly high EETs produced by the broken plate model indicate that this assumption is not valid. Therefore, the discussion below focuses on infinite plate models, similar to the previous research on the Western Interior and Laramide basins by Gao et al. (2016) and Lynds and Lichtner (2016).

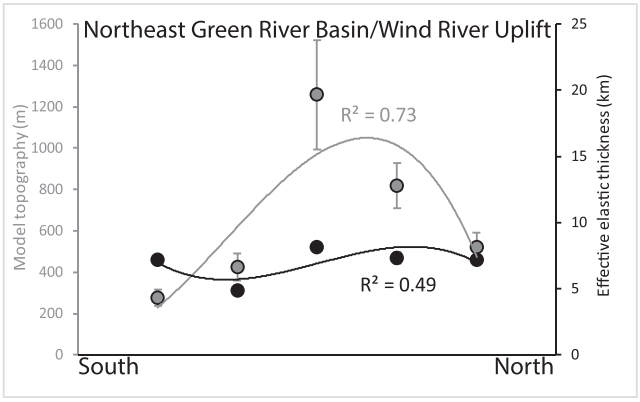

Figure 7. Along-strike variation in model load heights and effective elastic thickness on the south side of the Wind River uplift. Polynomial fits highlight that modeled topography (gray symbols) varies systematically by a factor of 6, with the greatest modeled topography in the center of the uplift and modeled topography tapering to the north and south. In contrast, effective elastic thickness (black symbols) is uniformly between 5 and 10 km, and variability is uncorrelated with modeled topography. Third-order polynomial regressions shown in both cases are intended only to highlight trends within each data set.

5.1. Topographic Loads

Effective elastic thickness and load height vary linearly with distance between the load and the control points (Figure S26). However, we find that even significant uncertainties (i.e., ≤10 km) in the relative position of the load and control points yields EET and load heights that are within 2σ uncertainty of the mean value.

Sensitivity analysis shows that the estimates of EET are not significantly impacted by the three-dimensional nature of uplifts (Figure 7). Furthermore, model results conform to theoretical predictions with the greatest topographic height in the center of the load. For example, in

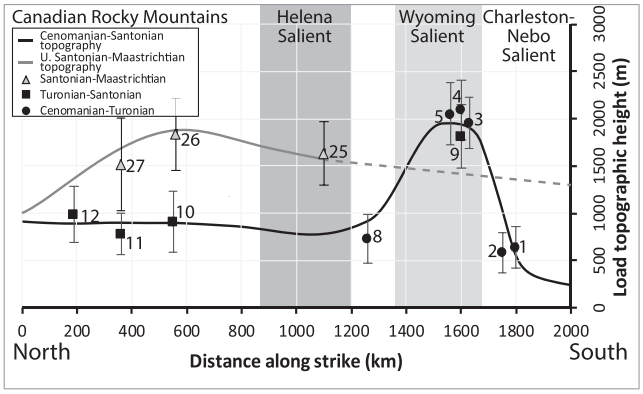

Figure 8. Modeled along-strike topographic evolution of the Sevier fold-thrust belt shows a northward migration of topographic growth. Cenomanian–Turonian and Turonian–Santonian topographic growth is focused in the Wyoming salient and decreases to the north and south. Santonian–Maastrichtian topographic growth is focused in the Canadian Rocky Mountains and decreases southward into the Helena salient. Numbers adjacent to data points correlate to profile locations in Figure 3.

the case of the Wind River Uplift modeled topography varies systematically by a factor of 6 from north to south. The greatest topographic height is in the center uplift and modeled topography tapers to the north and south. In contrast, effective elastic thickness is uniformly between 5 and 10 km, and variability is uncorrelated either with modeled topography or the location along strike.

Within the Sevier orogenic belt, the modeled magnitude of Cretaceous surface loading is variable along strike (Figure 8). The greatest (i.e., highest elevation) loads for Cenomanian–Santonian (~98–84 Ma) models are from the Wyoming Salient. Models from farther south, near the Charleston/Nebo/Pavant thrust systems, and north in the Helena Salient and Canadian Rocky Mountains, are characterized by smaller (i.e., lower elevation) loads (Figure 8). This changes for Santonian–Maastrichtian (~86–66 Ma) models, which show higher elevation in the Canadian Rocky Mountains and Helena Salient. Subsidence in Utah and Wyoming during the Campanian–Maastrichtian does not conform to a model of flexural due to loading by the Sevier orogenic belt (Kendall et al., 2019; Painter & Carrapa, 2013), and therefore an estimate of topographic loading during this interval is not possible.

Modeled topographic loading by Campanian–Maastrichtian (~77–66 Ma) uplifts in the foreland roughly increases from south to north, with the tallest modeled loads associated with the Granite Mountains and Laramie Range (42–43°N, Figures 9 and 10), although the correlation coefficient for this trend is very low. This northward increase in modeled topographic height is more pronounced and better correlated in the Paleocene–Eocene (Figure 9).

5.2. Effective Elastic Thickness

Estimates of EET display systematic temporal and spatial variations. Modeled EET decreases to the west, toward the paleocontinental margin and orogenic belt (Figure 11). When we plot predicted EET values relative to the distance east from the contemporary thrust belt, a general trend of increasing EET to the east is evident for the Cenomanian–Santonian (~98–84 Ma), Campanian–Maastrichtian (~77–66 Ma), and Paleocene–Eocene (~66–34 Ma) time intervals (Figure 11). Results show a regional decrease in EET after the Santonian (< ~84 Ma). Comparing profiles that are approximately the same distance from the Sevier thrust front, the EET for Campanian–Maastrichtian profiles is ~25–50% of the EET for Cenomanian–Santonian profiles (e.g., between 0–300 km from the thrust front, Figure 11). The Paleocene–Eocene models also show a decrease in EET relative to Campanian–Maastrichtian models between 200–450 km from the coeval thrust front (particularly Profiles 28 and 29 from the Piceance Basin and 37 from the Wind River Basin, Figure 11). This may be due to the lower reliability of the Paleocene-Eocene stratigraphic framework (see section 6.1 below).

6. Discussion

6.1. Uncertainties in Flexural Models

All models are affected to some degree by the datum correction for sediment accumulation that is unrelated to flexure (Table S3). Of the 39 modeled profiles in the United States and Canadian Western Interior, 20 have significant (i.e., >10% of maximum deflection) datum corrections to the modeled profile. Of these, eight (all Cenozoic profiles except 29, 30, and 32) are Paleocene–Eocene profiles from nonmarine basins. These basins are interpreted to be ponded or enclosed by uplifts (Dickinson et al., 1988). Such a structural restriction facilitates the vertical aggradation of fluvial, alluvial, and lacustrine deposits. Some Laramide basins had extensive restricted hydrology, evidenced by large Paleocene (Wind River Basin) and Eocene (Green River, Uinta, and Piceance basins) lacustrine systems (Smith et al., 2008). A large number of Cenozoic profiles required a datum correction; this is associated with greater scatter and uncertainty in the reconstructed EET. Profiles from the Green River, Uinta, and Piceance basins with large datum corrections are adjacent to profiles

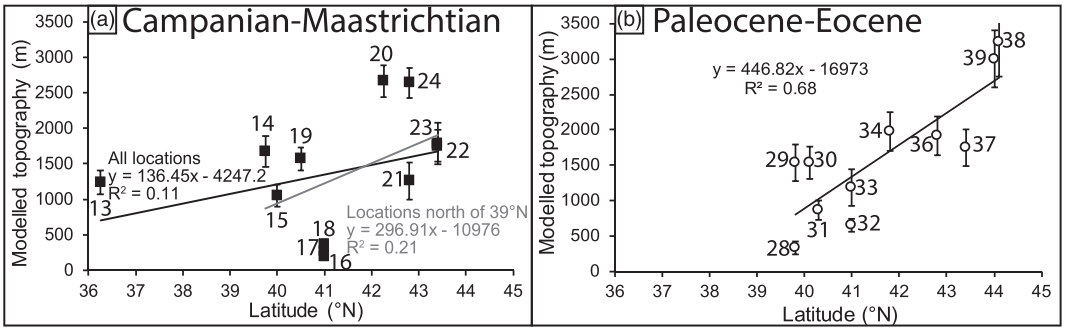

Figure 9. Comparison of topographic height of model loads in the (a) Campanian–Maastrichtian and (b) Paleocene–Eocene. Linear trends highlight the northward increase in modeled topography in both time intervals, and also highlight the increase in magnitude of uplift and northward gradient in uplift in the Cenozoic relative to the Cretaceous. Numbers adjacent to data points correlate to profile locations in Figure 3.

with low datum corrections. Despite the difference in datum corrections, these profiles yield comparable EET estimates. Moreover, Gao et al. (2016) found similar EET and trends for Wyoming, based on one Maastrichtian and nine Paleocene–Eocene profiles, and we therefore consider the Late Cretaceous–Paleogene conclusions robust.

Although changing the horizontal distance between the control points and load changes both the EET and load height, our analysis indicates that significant displacement (i.e., >10 km) is needed to change EET and load heights by more than their associated 2σ uncertainty (Figure S26). The temporal and spatial variation in modeled EET discussed below exceed the modeled 2σ uncertainty. Hence, we rule out uncertainty in the horizontal location of the control points as the cause of those changes.

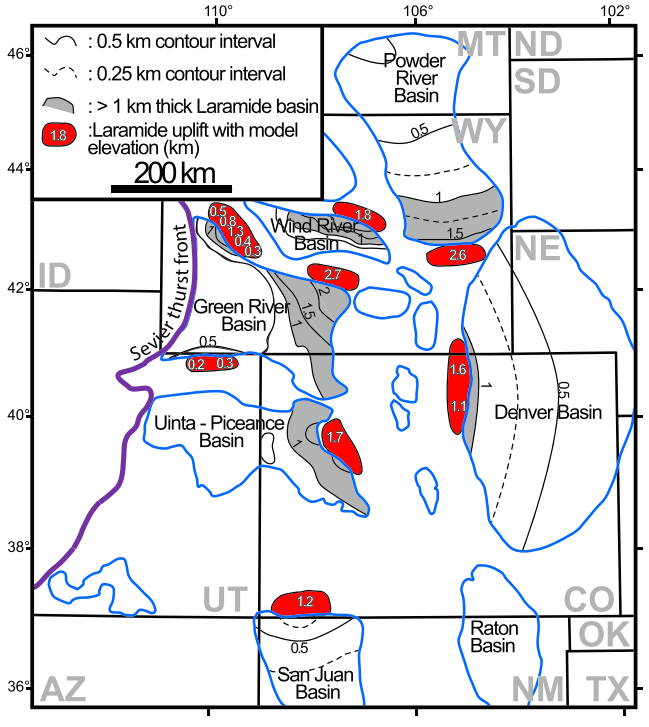

Figure 10. Distribution of sedimentary thicknesses in Maastrichtian Laramide basins and modeled topography. Abbreviations: AZ, Arizona; CO; Colorado; ID, Idaho; NE, Nebraska; ND, North Dakota; NM, New Mexico; MT, Montana; OK, Oklahoma; SD, South Dakota; TX, Texas; WY, Wyoming.

Sensitivity analysis of the along-strike changes in EET and load height for the Wind River Uplift indicates that load height is significantly impacted by the Uplift's three-dimensional geometry (Figure 7). However, EET is not similarly affected. We therefore consider our conclusions below regarding changes in EET to be more robust than those related to relief generation.

We assumed the top of all profiles to be flat, that is, without topographic or bathymetric relief. This assumption has only a minor effect on the analysis. For example, using a topographic-bathymetric slope of 0.03° (as found in modern systems), would cause about 50 m of elevation change for a 100 km profile. This small deflection is insufficient to explain the large differences in topographic height of the modeled loads. EET estimates are unaffected by this assumption because EET is determined by the wavelength of the deflection, rather than its magnitude.

EET estimates are dependent on the quality of the input stratigraphic profiles. Most profiles are based on reliable stratigraphic correlations, tied to good chronostratigraphic control, with maps based on hundreds of wells. Others are from a single published stratigraphic cross-section. Overall, stratigraphic correlations in Paleocene–Eocene sections are the most problematic, with limited paleontology and often erosion of the most proximal portions of the basin adjacent to the uplift. The reliability of the stratigraphic framework is the most important control in the quality specified in Table S1.

With a few exceptions, the discussion below focuses on trends between and within groups of flexural profiles and is therefore minimally reliant on the results of a particular profile which may be subject to the uncertainties described above. The consistent trends in EET and load heights

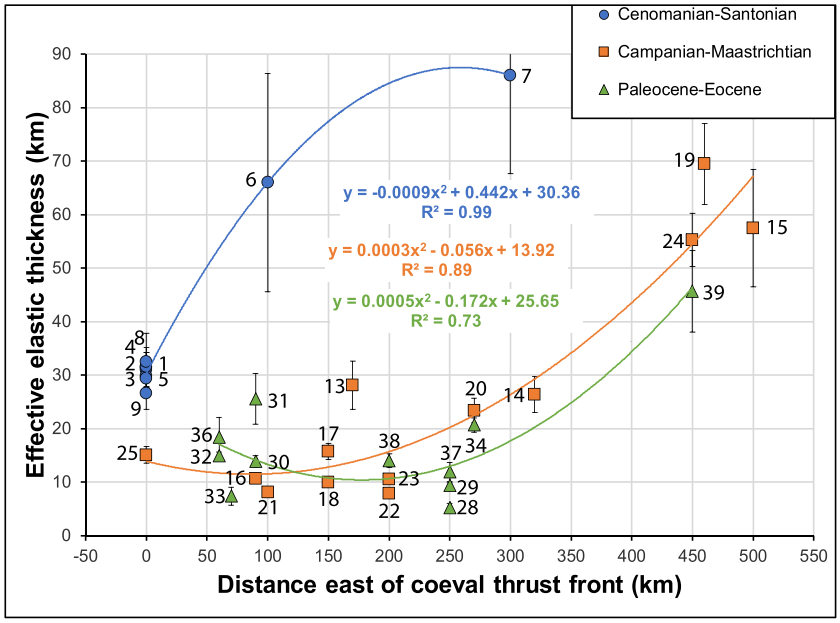

Figure 11. Comparison of effective elastic thickness relative to distance from the coeval Sevier thrust front shows that there is a westward decrease in effective elastic thickness in both the Late Cretaceous and Cenozoic. There is also a regional decrease in effect elastic thickness between the Cenomanian–Turonian and Campanian–Maastrichtian. There is only minor subsequent decrease between the Campanian–Maastrichtian and the Paleocene–Eocene. Second-order polynomial regressions shown are intended only to highlight variation between data sets. Numbers adjacent to data points correlate to profile locations in Figure 3.

between adjacent locations, and the similarity between our findings and previous work, suggest that the results of our analysis are robust to a first order.

6.2. Geodynamic Drivers of Uplift and Subsidence

In sections 6.2.1 and 6.2.2 we compare the timing and magnitude of modeled topographic loading to the thermochronologically determined timing of exhumation and paleoelevation estimates based on stable isotopic analyses. This leads to an evaluation of geodynamic models for uplift and subsidence in section 6.2.3. The comparison shows close correlation both in the timing of exhumation and the magnitude of topographic loading, confirming that flexural modeling can provide insight into the evolution of the load, the basin, and the lithosphere. Whereas stable isotope paleoelevation estimates are a snapshot of elevation that integrates all surface uplift until that time, flexurally modeled topography represents the topographic growth between discrete points in time. Flexural modeling also only yields topography above a base level (i.e., relief) rather than absolute elevation and will result in an underestimate of absolute elevation in the case of a nonmarine base level. Both of these effects will result in flexurally modeled relief which typically underestimates stable isotope paleoelevation reconstructions. The discussion below does not encompass the Hannah Basin because this basin has long been recognized as anomalously deep, and likely not primarily driven by flexural subsidence (Matson & Magathan, 2017). Rather, it is attributed to multiple subsidence mechanisms including block rotation and sediment loading (Lefebre, 1988).

6.2.1. Cordilleran Thrust Belt

Cenomanian–Turonian (~98–91 Ma) topographic growth in the Wyoming Salient (Figure 8) coincided with structural exhumation of major loads associated with motion on the Willard-Paris-Meade thrust system between 125 and 90 Ma (see Figure 3c for locations) (Coogan, 1992; DeCelles, 1994; Eleogram, 2014; Yonkee et al., 1989; Yonkee & Weil, 2015). This thrust system carries 10–15 km of Proterozoic through upper Paleozoic-age passive margin strata in its hanging wall and likely provided the topographic load to drive flexural subsidence. Subsidence may have been further enhanced by initial development of the Wasatch anticlinorium (see Figure 3c for location) (Giallorenzo, 2013; Yonkee & Weil, 2015). This deformation overlaps in time with emplacement of the Sheeprock and Canyon Range thrusts in central Utah (see Figure 3c for location) (DeCelles & Coogan, 2006). However, flexural modeling indicates that the latter

two did not induce as much subsidence south of the Uinta Mountains as the Willard-Paris-Meade system did to the north.

Continued elevated topography during emplacement of the Wasatch anticlinorium starting at the end of the Turonian is consistent with the critical taper model proposed by DeCelles and Mitra (1995). In that model, increased taper drove the orogenic wedge into a supercritical state and led to eastward propagation of the thrust front resulting in movement on the Crawford, Absaroka, and Hogsback thrusts between 90 and 50 Ma (see Figure 3c for location) (DeCelles, 1994; DeCelles & Mitra, 1995). Flexural modeling results from this study suggest there was no change in topographic load (i.e., no change in critical taper angle alpha) between the Turonian and Santonian (~94–84 Ma, Figure 8), implying that the transition to a supercritical state was caused by an increase in angle of the basal decollement (i.e., an increase in critical taper angle beta). Such an increase is consistent with impingement of the thrust system on the basement step at the Wasatch Hinge Zone, where Proterozoic metamorphic rocks are incorporated into the thrust belt to form the Wasatch aniclinorium (Camilleri et al., 1997; Yonkee, 1992). Our results and conclusions imply that emplacement of the Willard-Paris-Meade thrust system and initial shortening in the Wasatch anticlinorium created a similar crustal load to subsequent internal shortening in the Wasatch anticlinorium needed to maintain orogenic taper (DeCelles, 1994; Yonkee & Weil, 2015).

In contrast, post-Santonian (< ~84 Ma) strata from the Uinta and Green River basins (Figure 3) do not record a flexural foredeep attributable to loading by the Sevier fold-thrust belt (e.g., Kendall et al., 2019; Painter & Carrapa, 2013). This indicates a fundamental change in the geodynamic mechanism of subsidence after initial emplacement of the Wasatch anticlinorium. Possible explanations include (1) movement on the Crawford, Absaroka, and Hogsback thrusts provided insufficient topographic loading to produce flexure; (2) erosional unloading of thrust-belt topography resulted in unconformity development in the wedgetop and proximal foredeep depozones (Heller et al., 1988; Sinclair et al., 1991); or, more likely, (3) that topographic loading was compensated at depth, possibly due to uplift associated with flat subduction (Bishop et al., 2018; Dávila & Lithgow-Bertelloni, 2015; Flament et al., 2015) as previously suggested for Uinta Basin (Bartschi et al., 2018; Kendall et al., 2019). A possible exception is the Crazy Mountain Basin in southwestern Montana, which preserves stratal thickening adjacent to the thrust belt (Figure 3c). Here, over 2 km of Maastrichtian sediment are in proximity to the Helena Salient (see Figure 3 for location). Ongoing flexural subsidence in the Crazy Mountain Basin is consistent with its location at the boundary between the Laramide province and the simple foreland of the Western Canada Basin.

The increase in modeled thrust-belt topographic loads during the Santonian–Maastrichtian (~86–66 Ma) in the Helena Salient and the Canadian Rocky Mountains (Figure 8) also coincides with movement on major thrust systems in these regions. Unlike the Wyoming Salient, Late Cretaceous motion on thrusts in the Helena Salient and Canadian Foreland-Fold and Thrust Belt was focused in the late Santonian–Maastrichtian (Hardebol et al., 2007; Pană & van der Pluijm, 2015). In the Helena Salient, this included emplacement of several km of Proterozoic–early Paleozoic rocks over a major crustal ramp along the Lewis thrust between 83 and 75 Ma (Fuentes et al., 2012), and movement on the Jefferson Canyon-Lombard fault after 77 Ma (see Figure 3c for locations) (Harlan et al., 2008). In the Canadian foreland-fold and thrust belt, the Lewis thrust system deforms and therefore postdates Turonian strata (< ~90 Ma) (Larson & Price, 2006; Price, 1994). Emplacement of the linked Lewis-Bourgeau thrust system spanned 85–59 Ma (Simony & Carr, 2011), with a major pulse in the Campanian (Feinstein et al., 2007; Pană & van der Pluijm, 2015; van der Pluijm et al., 2006). These interpretations are consistent with previous attribution of Campanian–Maastrichtian foreland subsidence to enhanced flexural loading (Fanti & Catuneanu, 2010; Pană & van der Pluijm, 2015).

Modeled relief from the Late Cretaceous Canadian Rocky Mountains is 2.8 ± 0.5 km (sum of Profiles 10 and 26). There are few previous estimates of Late Cretaceous paleoelevation estimates for southern British Columbia. Fan and Dettman (2009) estimated paleoelevation of 4.3 ± 1.0 km by comparing the oxygen isotope composition paleosol carbonates which record in situ, low-elevation precipitation to carbonate from bivalves that lived in rivers interpreted to drain high elevations. Paleoelevation estimates are available from Eocene strata in the orogenic hinterland in southern British Columbia. These paleoelevation estimates, which are based on stable isotope compositions of carbonates, volcanic glass, and shear zone micas, and paleoflora analysis range from 2.2–4.9 km (Foster-Baril, 2017; Mix et al., 2011; Mulch et al., 2007; Smith

et al., 2009). Common to all previous estimates is a reliance on proxies that are dependent on isotopic lapse rates, precipitation amounts, or temperature and so may be influenced by climate change. The flexural modeling-based results therefore provide an independent estimate of Late Cretaceous paleoelevation and favor intermediate paleoelevations in the Late Cretaceous.

6.2.2. Laramide Province

6.2.2.1. Powder River and Bighorn Basins

Apatite fission track (AFT) ages in the Laramie range document Late Cretaceous (82–65 Ma) exhumation, but lack any evidence for younger, Cenozoic exhumation (Cerveny, 1990; Peyton & Carrapa, 2013). This is consistent with topographic growth based on flexural modeling which shows a single Late Cretaceous episode of development of topography in the Laramie range, but none in the Cenozoic. Cenozoic subsidence in the Powder River Basin is interpreted to be driven by exhumation of the Bighorn Range to the west. Fan and Dettman (2009) concluded that the late Paleocene Bighorn Range was at a paleoelevation of 4.5 ± 1.3 km, which is comparable to the flexurally modeled topographic relief of 3.2 ± 0.5 km. The data set presented here does not discriminate between earlier or later uplift of the Bighorn Range relative to the Beartooth Range (Cerveny, 1990; Omar et al., 1994; Peyton & Carrapa, 2013; Peyton et al., 2012), but it is consistent with a single episode of latest Cretaceous–Cenozoic exhumation in both cases.

6.2.2.2. Wind River and Northern Green River Basins

The cumulative topographic loading of 3.5 ± 0.5 km between the Campanian and Eocene documented in the Wind River Basin (Profiles 22, 23, and 36) and attributed to the Owl Creek Uplift is comparable to the 3.4 ± 0.7 km elevation calculated based on stable isotope paleoelevation (Fan et al., 2011). Similarly, the cumulative loading of 3.2 ± 0.4 km documented in the NW Green River Basin and attributed to the Wind River Uplift (Profiles 21 and 37) is within uncertainty of the paleoelevation estimated by Fan et al. (2011). Fan et al. (2011) attribute this entire uplift event to the lower Eocene boundary between the Indian Meadows and Wind River formations (~54.5–53 Ma). However, AFT ages from the Wind River Uplift document cooling in the Campanian–Paleocene (Cerveny & Steidtmann, 1993; Fan & Carrapa, 2014; Peyton & Carrapa, 2013; Peyton et al., 2012). Combined with the subsidence pattern from the adjacent Green River Basin, this suggests that topography in the Wind River Range likely grew more slowly during the Late Cretaceous, with more rapid growth in the Paleocene–early Eocene. We conclude that the stable isotopic compositions observed by Fan et al. (2011) accurately reflect the topography of the mountains surrounding the basin, but that the timing of the isotopic shift is likely due to a change in fluvial networks (i.e., a provenance change) rather than directly recording the timing of attainment of high elevations. Campanian AFT ages from the Granite Mountains in the northeastern Green River Basin support that exhumation was ongoing in the Maastrichtian, consistent with the model results (Cerveny, 1990). However, the lack of additional thermochronology or paleoelevation research limits further comparison of this uplift to model results.

6.2.2.3. Southern Green River Basin

In the southwest Green River Basin, flexural modeling indicates that surface loading by the Uinta Mountains increased from ~200–400 m in the Campanian to ~1,200 m in the Paleocene–early Eocene before reducing again to ~650 m in the late Eocene. Preliminary development of topography in the Campanian is consistent with northward-oriented paleoflow indicators from the Campanian Ericson Sandstone exposed on the north flank of the Uinta Mountains (Leary et al., 2015) and with a cessation of delivery of detritus derived from north of the Uinta Mountains to the Book Cliffs area (Bartschi et al., 2018). The major increase in relative topography between the Late Cretaceous and Paleogene is also consistent with the findings of Gao and Fan (2018) based on a decrease in $\delta^{18}O$ values of carbonate cement in sandstones. Their record provides greater resolution than our flexural modeling and indicates that the increase in elevation occurred between the lower Paleocene lower Fort Union Formation and the upper Paleocene upper Fort Union Formation or Eocene Wasatch Formation. Nevertheless, the cumulative relative elevation gain between the Late Cretaceous and Eocene of ~2.1 ± 0.4 km (estimated from Profiles 16, 17, 33, and 34) is within uncertainty of the 2.5 ± 1.2 km estimated based on stable isotope paleoaltimetry (Gao & Fan, 2018).

6.2.2.4. Piceance Basin

AFT ages from the White River Uplift indicate rapid cooling between 63 and 34 Ma (Landman & Flowers, 2013; Naeser et al., 2002; Peyton & Carrapa, 2013), consistent with the observed Paleocene–Eocene subsidence. However, there is no thermochronologic evidence for an earlier, Maastrichtian episode of loading which is documented in the subsidence record of the Piceance Basin (profile 14). There are several potential explanations for this anomaly. The first is that exhumation related to Rio Grande rifting (Naeser

et al., 2002) or regional Neogene dynamic uplift due to mantle upwelling documented by anomalously low seismic velocities (the Aspen and San Juan anomalies) (Karlstrom et al., 2012; Kelley et al., 2010) resulted in erosion of rocks recording the earlier exhumation history. Alternatively, Late Cretaceous subsidence may have been driven by exhumation to the east of the White River Uplift, such as the Park Range which does document Maastrichtian exhumation (Cerveny, 1990; Kelley, 2005).

6.2.2.5. Denver Basin

AFT ages and models indicate that the onset of exhumation in the Front Range began in the Campanian, consistent with subsidence modeling (Bryant & Naeser, 1980; Kelley & Chapin, 1997; Kelley & Chapin, 2004; Naeser et al., 2002). AFT models indicate that the exhumation continued into the Cenozoic. However, south of ~39.75°N (i.e., south of Denver) the AFT partial annealing zone is preserved along the eastern Front Range (Kelley & Chapin, 2004). This suggests that there has been less exhumation along the range front to the south than to the north, consistent with the decreased magnitude of subsidence during the Eocene relative to the Campanian–Maastrichtian (Raynolds, 2002).

6.2.2.6. Laramide Summary

Consistency among the thermochronologically determined timing of exhumation, the magnitude of surface uplift based on stable isotope paleoaltimetry, and development of topography based on flexural modeling lends confidence that modeling produces reasonable constraints on paleotopography. While determining surface loading based on flexural modeling has inherent caveats (e.g., Royden, 1993), flexural modeling provides an independent method that compliments techniques of structural restoration, thermochronology, paleoaltimetry, and basin modeling.

6.2.3. Geodynamic Models of Uplift and Subsidence

Modeled topography shows two stages of uplift, consistent with the observations of Fan and Carrapa (2014): slow uplift and exhumation in the Campanian–Maastrichtian and more rapid uplift and exhumation in the Paleocene–Eocene. Below we summarize these new results and compare them with previously published work to evaluate models for Laramide uplift and basin formation. In both the Campanian–Maastrichtian (~77–66 Ma) and the Paleocene–Eocene (~66–34 Ma), modeled loads in the Laramide province increased from south to north, but the uplift gradient is greater and uplift was better correlated with latitude in the Paleocene–Eocene (Figure 9). During the Campanian–Maastrichtian the greatest loads were associated with the Granite Mountains, Owl Creek Mountains, and Laramie Range (Figures 9 and 10). Based on modeling, the greatest Paleocene–Eocene loads were associated with the Beartooth and Bighorn uplifts. Liu et al. (2010) predict a northward migration of a zone of dynamic subsidence associated with north-northeast directed subduction of a conjugate Shatsky Rise. Their model predicts that the region north of 40°N should have transitioned from absolute uplift to absolute subsidence between the Campanian–Maastrichtian and Paleocene, which is the opposite of what is observed in the flexural model-based topography. Heller and Liu (2016) modified the conclusions of Liu et al. (2010) by comparing the rate of uplift or subsidence to geological phenomena in the western United States. Although the timing of the transition from relative subsidence to relative uplift matches that observed in the flexure-based topography model, the geographic pattern does not. Specifically, the model of Heller and Liu (2016) predicts roughly coeval along-strike (i.e., north–south) uplift or subsidence and predicts significant east-west variability in the timing of uplift. It does not account for the along-strike variability or northward increase in uplift seen in both Late Cretaceous and Paleogene flexural models. Rather, the pattern of uplift observed in the flexural models appears consistent with (1) minor Late Cretaceous–early Paleocene uplift at the front of a flat slab due to accumulation of bulldozed buoyant continental mantle lithosphere (Axen et al., 2018) followed by (2) late Paleocene–early Eocene rollback of the flat slab (Coney & Reynolds, 1977; Constenius et al., 2003; Copeland et al., 2017; Liu & Gurnis, 2010) which would induce uplift by both isostatic (Humphreys, 2009; Kay & Coira, 2009) and nonisostatic (Buiter et al., 2002; Liu & Gurnis, 2010; Moucha et al., 2008) mechanisms. Rollback can also drive crustal shortening as the downgoing plate pulls crustal material into the zone above the rollback hinge, and isostatic rebound following removal of eclogitized lower crust (Axen et al., 2018) similar to mechanisms associated with delamination of continental lithosphere (Göğüş & Pysklywec, 2008; Krystopowicz & Currie, 2013).

6.3. Temporal Evolution of Effective Elastic Thickness

Comparison of estimates of modern and Late Cretaceous–Paleogene EET of the North American Cordillera indicates that the modern distribution of EET evolved by the Campanian–Maastrichtian (~77–66 Ma). In the Laramide province (i.e., south of ~48°N) EET estimates for the Cenomanian–Santonian (~98–84 Ma) are

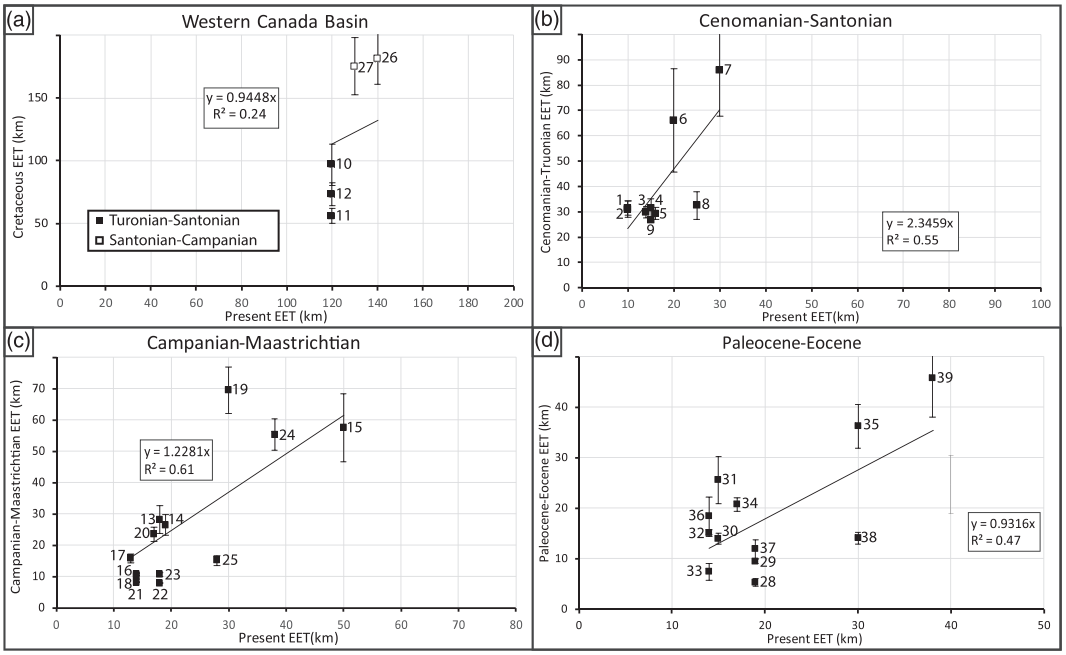

Figure 12. Comparison of effective elastic thicknesses through time to modern effective elastic thickness. (a) Effective elastic thickness in the Western Canada Basin is high in the Turonian–Santonian and increases to near-modern values by the Santonian–Campanian. (b) Cenomanian–Turonian effective elastic thicknesses are more than twice modern. (c) Campanian–Maastrichtian and (d) Paleocene–Eocene effective elastic thicknesses are comparable to modern. All linear fits were forced through the origin. Numbers adjacent to data points correlate to profile locations in Figure 3.

approximately 2 times modern EET estimates (Figure 12b). In contrast, Campanian–Maastrichtian EET estimates are roughly the same as modern EET (Figure 12c). Paleocene–Eocene EET estimates are slightly lower than modern EET estimates (Figure 12d), consistent with the additional weakening noted above (Figure 11) and by Gao et al. (2016). We conclude that a significant weakening of the North American lithosphere occurred between the Santonian and Campanian (i.e., between ~84 and 77 Ma), and minor additional weakening between the Cretaceous and Paleogene. The lower EET in the Paleocene–Eocene relative to the modern EET may suggest that there has been some stiffening of the lithosphere via deepening of the lithosphere-asthenosphere boundary or thermal or rheological strengthening of the lithosphere since the Eocene (Burov & Diament, 1995).

During the interval that the lithosphere of the Laramide province was undergoing significant weakening, the lithosphere beneath the Western Canada Basin underwent a moderate increase in EET from ~70 km to >100 km (Figure 12a). Following this increase in EET, Santonian–Campanian EETs were extremely thick and comparable to modern EETs. We conclude that processes responsible for the decrease in EET in the Laramide province did not affect the Western Canada Basin.

6.4. Mechanisms for Weakening the Upper Plate

At least four groups of mechanisms have been proposed to drive weakening of the North American lithosphere: (1) heating of the upper plate as a result of the inboard sweep of volcanism associated with shallowing of the subduction angle; (2) heating of the upper plate due to magma generation following slab steepening; (3) bulldozing of weak lower lithosphere followed by hydration of the North American lithosphere during flat subduction; and (4) a combination of (a) bending stresses due to the Sevier topographic load, (b) decoupling of the crust and mantle, and (c) end-loading of the North American plate during flat subduction. We discuss these hypotheses in light of the new constraints on the temporal and spatial distribution of lithospheric strength below.

Weakening of the North American plate due to heating of the upper plate associated with an inboard sweep of Laramide arc-volcanism related to flat slab advance (Figure 2a) is inconsistent with the temporal and spatial trends in weakening determined from flexural modeling. This mechanism would result in weakening that was coeval with and progressed inboard at the same rate as the advancing slab. The most recent reconstruction shows that the inboard sweep of magmatism would have begun by ~100 Ma, reached the Laramide province between 100–80 Ma, and reached its inboard-most location at ~52 Ma (Constenius et al., 2003; Copeland et al., 2017). However, at the resolution available based on flexural modeling, there is no spatial diachroneity in the decrease of EET in the Late Cretaceous. Rather, the regional reduction in the strength of the lithosphere affected all locations modeled in this study between the Santonian and Campanian (i.e., between ~84 and 77 Ma). There was only a minor decrease in EET between the Maastrichtian and Paleogene between 200–450 km from the Sevier thrust front (Figure 11). Our conclusions are similar to those of Gao et al. (2016), who found that EET within the Wyoming segment of the Laramide province decreased spatially to the west, but whose data lacked the temporal spread to observe a trend.

Weakening due to lithospheric heating following removal of the flat slab (Figure 2b) is also inconsistent with the timing of weakening determined from flexural modeling. This hypothesis predicts that weakening should postdate slab steepening. Whereas the most significant weakening based on flexural modeling occurred between the Santonian and Campanian (i.e., between ~84 and 77 Ma), the slab did not begin to resteepen until the Eocene (Constenius et al., 2003; Copeland et al., 2017). Furthermore, the consistency between the Late Cretaceous and modern distribution of EET suggests that heating due to the Paleogene magmatic flare-up had little effect on the bulk strength of the lithosphere.

Bulldozing and hydration of the North American lithosphere during flat subduction (Figure 2c) provides a partial explanation for upper plate weakening because it is consistent with the timing and extent of weakening of the North American lithosphere. Bulldozing may have removed the weak lower lithosphere (Axen et al., 2018), maximizing lithospheric weakening by direct hydration of strong lithospheric material. In the inverse convection model of Liu et al. (2010) the crest of the shallowly subducting Farallon plate (defined as the 179 km contour) arrives in the SW portion of the Laramide province between 88 and 80 Ma: coincident with the timing of the primary reduction in lithospheric strength based on flexural modeling (Figure 11). The lithospheric mantle at depths of 70–150 km below North America currently has anomalously low *S* wave velocities, which may reflect hydration-induced weakening (Sommer & Gauert, 2011; Van Der Lee & Frederiksen, 2005). The extent of the weak lithospheric mantle inferred from *S* wave velocities correlates to the regions of low Late Cretaceous EET identified flexural modeling as well as low modern EET (Tesauro et al., 2015). Additional Paleogene weakening in the core of the Laramide province (Figure 11) may have been due to additional hydration during ongoing flat subduction. Hydration of the lithosphere may also decrease its density (Humphreys et al., 2003), causing broad uplift and potentially contributing to the demise of the flexural foreland basin in western Wyoming in the Campanian (Painter & Carrapa, 2013).

The combined hypothesis that includes end-loading of the North American plate, bending stresses due to Sevier topographic loading, and decoupling of the crust and mantle (Figure 2d) also provides a partial explanation for the spatial and temporal trends in EET. For example, weakening due to end-loading alone should have coincided with transmission of stresses due to the initiation of flat subduction at 93–88 Ma (Saleeby et al., 2007), whereas it is not observed in flexural models until after 84 Ma. Bending stresses due to Sevier topographic loading may explain the westward decrease in EET observed in all time slices (Figure 11), but this could also be explained by weakening approaching the attenuated paleocontinental margin. It is unclear what would drive decoupling of the crust and mantle as there is no evidence for regional crustal thickening (as opposed to crustal thickening associated with discreet faults) in the Laramide province in the Campanian–Maastrichtian.

We propose that the sudden Campanian decrease in Cordilleran EET is best explained by weakening as a result of bulldozing and hydration of the lithosphere. In this scenario, initiation of compressional stress throughout the upper plate due to end-loading associated with the onset of flat subduction (Axen et al., 2018; Livaccari & Perry, 1993) may have driven early minor deformation in the Laramide province (Carrapa et al., 2019). Later weakening driven by bulldozing and hydration focused stress and strain above the weakened lithosphere, resulting in the onset of significant deformation in the Laramide province. Uplift of the proximal (western) foreland basin and development of several tectonic unconformities in the

Campanian (Moxa unconformities 1 and 2, Rudolph et al., 2015) is consistent with isostatic uplift due to a decrease in density of the lithosphere associated with hydration (Humphreys, 2009; Humphreys et al., 2003) or uplift over the crest of the flat slab (Dávila et al., 2010; Dávila & Lithgow-Bertelloni, 2015; Eakin et al., 2014; Espurt et al., 2010; Jadamec et al., 2013; Kendall et al., 2019).

Weakening of the North American mantle lithosphere allowed individual Laramide structures to localize along preexisting crustal heterogeneities which may have served to further weaken the lithosphere. The Campanian–modern EET of the Laramide province is extremely low compared to theoretical considerations (e.g., Burov & Diament, 1996). This suggests that deformation may have further reduced the integrated strength of the lithosphere. This additional deformation-related weakening is supported by observations that modern EET estimates decrease from the center of the Green River Basin toward the basin-bounding faults (Lowry & Smith, 1994; Lowry & Smith, 1995).

7. Conclusions

Monte Carlo flexural modeling of Late Cretaceous–Eocene basin fill from Cordilleran foreland basins from New Mexico to southern Canada reveals both spatial and temporal variation in EET. Throughout the Late Cretaceous–Eocene, we observe an east-to-west decrease in EET. This spatial decrease in EET may be associated with either bending stresses associated with the Sevier thrust-belt, or increased proximity to attenuated continental crust at the paleocontinental margin.

Campanian–Maastrichtian focusing of Laramide deformation and basin formation was concurrent with and was caused by a sudden EET reduction. EET estimated from Campanian–Maastrichtian (~77–66 Ma) subsidence patterns are reduced by about half relative to Cenomanian–Santonian (~98–84 Ma) estimates. There may have been an additional, minor decrease in EET at the eastern edge of the Laramide province between the Maastrichtian and Paleocene–Eocene; the latter change in EET is however poorly resolved in our data set. In contrast, the lithosphere was much stronger in the Western Canada Basin, did not experience significant weakening as is seen to the south, and did not undergo Laramide deformation. This illustrates that in the absence of flat subduction, the upper plate did not weaken, and Laramide deformation did not occur.

The timing of the sudden decrease in EET is most consistent with weakening of the North American lithosphere by hydration following bulldozing of the lower lithosphere by a shallowly subducting Farallon slab. Hydration and the attendant weakening may have served to focus plate-wide contractional stress introduced by end-loading at the onset of flat subduction. Hydration and weakening of the North American lithosphere thus controlled both the spatial extent and timing of Laramide deformation. Laramide deformation, in turn, may have further reduced the EET by reducing the strength of the upper crust. Thus, the Laramide orogeny was, in part, a consequence of lithospheric weakening. The genetic linkage between flat slab subduction and the reduction in EET suggests that the extent of flat subduction can be mapped by changes in the EET in the Late Cretaceous.

Late Cretaceous, Paleogene, and Holocene EET values are similar in our study area, suggesting that the modern lithospheric structure was developed during Late Cretaceous flat subduction. This evolution profoundly changed the rheology of the western continent, and resulted in a physical state that approaches the present day in terms of the strength of the lithosphere.

Data Availability Statements

Data sets and results are available at this site (https://doi.org/10.5281/zenodo.3662883). Software is available at this site (https://doi.org/10.5281/zenodo.3662805).

Acknowledgments

This research was supported by grants from the National Science Foundation (EAR-1824557) and the University of British Columbia. We thank multiple colleagues, including G. J. Axen, C. A. Currie, and S. L. Peyton, for helpful discussions and comments. We are grateful to JGR Editor Isabelle Manighetti and the Associate Editor for their detailed comments on this manuscript. We thank an anonymous reviewer for their careful review.

References

Allen, P., & Allen, J. (2005). *Basin analysis: Principles and applications* (2nd ed., p. 549). Oxford: Blackwell scientific publications.

Armstrong, R. L. (1968). Sevier orogenic belt in Nevada and Utah. *Geological Society of America Bulletin*, *79*(4), 429. https://doi.org/10.1130/0016-7606(1968)79[429:sobina]2.0.co;2

Armstrong, R. L., & Ward, P. (1991). Evolving geographic patterns of Cenozoic magmatism in the north American cordillera: The temporal and spatial association of magmatism and metamorphic core complexes. *Journal of Geophysical Research*, *96*(B8), 13,201–13,224. https://doi.org/10.1029/91JB00412

Axen, G. J., van Wijk, J. W., & Currie, C. A. (2018). Basal continental mantle lithosphere displaced by flat-slab subduction. *Nature Geoscience*, *11*(12), 961–964. https://doi.org/10.1038/s41561-018-0263-9

Bartschi, N. C., Saylor, J. E., Lapen, T. J., Blum, M. D., Pettit, B., & Andrea, R. A. (2018). Tectonic controls on Late Cretaceous sediment provenance and stratigraphic architecture in the Book Cliffs, Utah. *Geological Society of America Bulletin*, *130*(11–12), 1763–1781. https://doi.org/10.1130/B31927.1

Bechtel, T. D., Forsyth, D. W., Sharpton, V. L., & Grieve, R. A. (1990). Variations in effective elastic thickness of the North American lithosphere. *Nature*, *343*(6259), 636–638. https://doi.org/10.1038/343636a0

Becker, T., & Lynds, R. (2012). A geologic deconstruction of one of the world's largest natural accumulations of CO_2, Moxa Arch, southwestern Wyoming. *AAPG Bulletin*, *96*(9), 1643–1664. https://doi.org/10.1306/01251211089

Becker, T. P., McGroder, M., Rudolph, K. W., Hauge, T. A., & Fan, M. (2010). Paleogene influence of the Moxa Arch on the architecture of the composite Darby-Hogsback-Prospect (DHP) thrust sheet near Labarge, Wyoming, USA, in *AAPG Annual Conference and Exhibit*, Edited, New Orleans, LA.

Best, M. G., Barr, D. L., Christiansen, E. H., Gromme, S., Deino, A. L., & Tingey, D. G. (2009). The Great Basin Altiplano during the middle Cenozoic ignimbrite flareup: Insights from volcanic rocks. *International Geology Review*, *51*(7–8), 589–633. https://doi.org/10.1080/00206810902867690

Bills, B. G., & May, G. M. (1987). Lake Bonneville: Constraints on lithospheric thickness and upper mantle viscosity from isostatic warping of Bonneville, Provo, and Gilbert stage shorelines. *Journal of Geophysical Research*, *92*(B11), 11,493–11,508. https://doi.org/10.1029/JB092iB11p11493

Bird, P. (1988). Formation of the Rocky Mountains, Western United States: A continuum computer model. *Science*, *239*(4847), 1501–1507. https://doi.org/10.1126/science.239.4847.1501

Bishop, B. T., Beck, S. L., Zandt, G., Wagner, L. S., Long, M. D., & Tavera, H. (2018). Foreland uplift during flat subduction: Insights from the Peruvian Andes and Fitzcarrald arch. *Tectonophysics*, *731–732*, 73–84. https://doi.org/10.1016/j.tecto.2018.03.005

Bonde, J. W., Hilton, R. P., Jackson, F. D., & Druschke, P. A. (2015). Fauna of the Newark canyon formation (Lower Cretaceous), East-Central Nevada. In W. Pennell & L. Garside (Eds.) *2015 Geological Society of Nevada Symposium* (pp. 139–150). Reno, NV: Nevada Geological Society.

Bryant, B., & Naeser, C. W. (1980). The significance of fission-track ages of apatite in relation to the tectonic history of the front and Sawatch ranges, Colorado. *GSA Bulletin*, *91*(3), 156–164. https://doi.org/10.1130/0016-7606(1980)91<156:Tsofao>2.0.Co;2

Buiter, S. J. H., Govers, R., & Wortel, M. J. R. (2002). Two-dimensional simulations of surface deformation caused by slab detachment. *Tectonophysics*, *354*(3–4), 195–210. https://doi.org/10.1016/S0040-1951(02)00336-0

Burchfiel, B., & Davis, G. A. (1972). Structural framework and evolution of the southern part of the Cordilleran orogen, western United States. *American Journal of Science*, *272*(2), 97–118. https://doi.org/10.2475/ajs.272.2.97

Burov, E. B., & Diament, M. (1995). The effective elastic thickness (T_e) of continental lithosphere: What does it really mean? *Journal of Geophysical Research*, *100*(B3), 3905–3927. https://doi.org/10.1029/94JB02770

Burov, E. B., & Diament, M. (1996). Isostasy, equivalent elastic thickness, and inelastic rheology of continents and oceans. *Geology*, *24*(5), 419–422. https://doi.org/10.1130/0091-7613(1996)024<0419:IEETAI>2.3.CO;2

Camilleri, P., Adolph Yonkee, W., Coogan, J., DeCelles, P., McGrew, A., & Wells, M. (1997). Hinterland to foreland transect through the Sevier Orogen, Northeast Nevada to north Central Utah: Structural style, metamorphism, and kinematic history of a large contractional orogenic wedge. *Brigham Young University Geology Studies*, *42*, 297–309.

Carrapa, B., DeCelles, P. G., & Romero, M. (2019). Early inception of the Laramide orogeny in southwestern Montana and northern Wyoming: Implications for models of flat-slab Subduction. *Journal of Geophysical Research: Solid Earth*, *124*, 2102–2123. https://doi.org/10.1029/2018JB016888

Catuneanu, O., Beaumont, C., & Waschbusch, P. (1997). Interplay of static loads and subduction dynamics in foreland basins: Reciprocal stratigraphies and the "missing" peripheral bulge. *Geology*, *25*(12), 1087–1090. https://doi.org/10.1130/0091-7613(1997)025<1087:Ioslas>2.3.Co;2

Cerveny, P. III (1990). Fission-track thermochronology of the wind river range and other basement-cored uplifts in the Rocky mountain foreland., Wyoming Univ., Laramie, WY (United States).

Cerveny, P. F., & Steidtmann, J. R. (1993). Fission track thermochronology of the Wind River range, Wyoming: Evidence for timing and magnitude of Laramide exhumation. *Tectonics*, *12*(1), 77–91. https://doi.org/10.1029/92TC01567

Clinkscales, C. A., & Lawton, T. F. (2014). Timing of Late Cretaceous shortening and basin development, Little Hatchet Mountains, southwestern New Mexico, USA—Implications for regional Laramide tectonics. *Basin Research*. https://doi.org/10.1111/bre.12083

Coney, P. J. (1980). Cordilleran metamorphic core complexes: An overview. In M. D. Crittenden, P. J. Coney & G. H. Davis (Eds.), *Cordilleran metamorphic core complexes*, *Geological Society of America Memoirs* (Vol. 153, pp. 7–31). Boulder, CO: Geological Society of America. https://doi.org/10.1130/MEM153-p7

Coney, P. J., & Reynolds, S. J. (1977). Cordilleran Benioff zones. *Nature*, *270*(5636), 403–406. https://doi.org/10.1038/270403a0

Coney, P. J., Smith, R., & Eaton, G. (1978). Mesozoic-Cenozoic cordilleran plate tectonics, Cenozoic tectonics and regional geophysics of the western Cordillera. *Geological Society of America Memoirs*, *152*, 33–50. https://doi.org/10.1130/MEM152-p33

Constenius, K. N., Esser, R. P., & Layer, P. W. (2003). Extensional collapse of the Charleston-Nebo salient and its relationship to space-time variations in Cordilleran Orogenic Belt tectonism and continental stratigraphy. In R. G. Raynolds, & R. M. Flores (Eds.), *Cenozoic Systems of the Rocky Mountain Region* (pp. 303–353). Denver: Rocky Mountain SEPM.

Coogan, J. C. (1992). Structural evolution of piggyback basins in the Wyoming-Idaho-Utah thrust belt. In P. K. Link, M. A. Kuntz & L. B. Platt (Eds.), *Regional geology of eastern Idaho and western Wyoming* (Vol 179, Chap 2., pp. 55–81). Boulder, CO: Geological Society of America.

Copeland, P., Currie, C. A., Lawton, T. F., & Murphy, M. A. (2017). Location, location, location: The variable lifespan of the Laramide orogeny. *Geology*, *45*(3), 223–226. https://doi.org/10.1130/g38810.1

Currie, C. A., & Beaumont, C. (2011). Are diamond-bearing cretaceous kimberlites related to low-angle subduction beneath western North America? *Earth and Planetary Science Letters*, *303*(1–2), 59–70. https://doi.org/10.1016/j.epsl.2010.12.036

Dahlen, F. A. (1990). Critical taper model of fold-and-thrust belts and accretionary wedges. *Annual Review of Earth and Planetary Sciences*, *18*(1), 55–99. https://doi.org/10.1146/annurev.ea.18.050190.000415

Dahlstrom, C. D. (1970). Structural geology in the eastern margin of the Canadian Rocky Mountains. *Bulletin of Canadian Petroleum Geology*, *18*(3), 332–406.

Dávila, F. M., & Lithgow-Bertelloni, C. (2015). Dynamic uplift during slab flattening. *Earth and Planetary Science Letters*, *425*, 34–43. https://doi.org/10.1016/j.epsl.2015.05.026

Dávila, F. M., Lithgow-Bertelloni, C., & Giménez, M. (2010). Tectonic and dynamic controls on the topography and subsidence of the Argentine pampas: The role of the flat slab. *Earth and Planetary Science Letters*, *295*(1–2), 187–194. https://doi.org/10.1016/j.epsl.2010.03.039

DeCelles, P., Gray, M., Ridgway, K., Cole, R., Srivastava, P., Pequera, N., & Pivnik, D. (1991). Kinematic history of a foreland uplift from Paleocene synorogenic conglomerate, Beartooth range, Wyoming and Montana. *Geological Society of America Bulletin*, *103*(11), 1458–1475. https://doi.org/10.1130/0016-7606(1991)103<1458:KHOAFU>2.3.CO;2

DeCelles, P. G. (1994). Late Cretaceous-Paleocene synorogenic sedimentation and kinematic history of the Sevier thrust belt, Northeast Utah and Southwest Wyoming. *GSA Bulletin*, *106*(1), 32–56. https://doi.org/10.1130/0016-7606(1994)106<0032:LCPSSA>2.3.CO;2

DeCelles, P. G. (2004). Late Jurassic to Eocene evolution of the Cordilleran thrust belt and foreland basin system, western USA. *American Journal of Science*, *304*(2), 105–168. https://doi.org/10.2475/ajs.304.2.105

DeCelles, P. G. (2012). Foreland Basin systems revisited: Variations in response to tectonic settings. In C. Busby, & A. Azor (Eds.), *Tectonics of sedimentary basins* (pp. 405–426). Chichester: John Wiley & Sons, Ltd. https://doi.org/10.1002/9781444347166.ch20

DeCelles, P. G., & Coogan, J. C. (2006). Regional structure and kinematic history of the Sevier fold-and-thrust belt, Central Utah. *Geological Society of America Bulletin*, *118*(7–8), 841–864. https://doi.org/10.1130/b25759.1

DeCelles, P. G., & Giles, K. A. (1996). Foreland basin systems. *Basin Research*, *8*(2), 105–123. https://doi.org/10.1046/j.1365-2117.1996.01491.x

DeCelles, P. G., & Mitra, G. (1995). History of the Seveir orogenic wedge in terms of critical taper models, northeast Utah and Southwest Wyoming. *Geological Society of America Bulletin*, *107*(4), 454–462. https://doi.org/10.1130/0016-7606(1995)107<0454:hotsow>2.3.co;2

DeCelles, P. G., Tolson, R. B., Graham, S. A., Smith, G. A., Ingersoll, R. V., White, J., et al. (1987). Laramide thrust-generated alluvial-Fan sedimentation, Sphinx conglomerate, southwestern Montana1. *AAPG Bulletin*, *71*(2), 135–155.

DeSilva, S., Zandt, G., Trumbull, R., Viramonte, J. G., Salas, G., & Jimenez, N. (2006). Large ignimbrite eruptions and volcano-tectonic depressions in the Central Andes: A thermomechanical perspective. *Geological Society of London, Special Publication*, *269*(1), 47–63. https://doi.org/10.1144/GSL.SP.2006.269.01.04

Devlin, W. J., Rudolph, K. W., Shaw, C. A., & Ehman, K. D. (1993). The effect of tectonic and eustatic cycles on accommodation and sequence-stratigraphic framework in the Upper Cretaceous foreland basin of southwestern Wyoming. In H. W. Posamentier, C. P. Summerhayes, B. U. Haq & G. P. Allen (Eds.), *Sequence Stratigraphy and Facies Associations* (pp. 501–520). Oxford: Blackwell Publishing Ltd. https://doi.org/10.1002/9781444304015.ch25

Dickinson, W. R. (2013). Phanerozoic palinspastic reconstructions of Great Basin geotectonics (Nevada-Utah, USA). *Geosphere*, *9*(5), 1384–1396. https://doi.org/10.1130/ges00888.1

Dickinson, W. R., Klute, M. A., Hayes, M. J., Janecke, S. U., Lundin, E. R., McKittrick, M. A., & Olivares, M. D. (1988). Paleogeographic and paletotectonic seeting of Laramide sedimentary basins in the central Rocky-Mountain region. *Geological Society of America Bulletin*, *100*(7), 1023–1039. https://doi.org/10.1130/0016-7606(1988)100<1023:PAPSOL>2.3.CO;2

Dickinson, W. R., & Snyder, W. S. (1978). Plate tectonics of the Laramide orogeny. In V. Matthews (Ed.), *Laramide folding associated with basement block faulting in the western United States* (pp. 355–366). Boulder: Geological Society of America. https://doi.org/10.1130/MEM151-p355

Eakin, C. M., Long, M. D., Beck, S. L., Wagner, L. S., Tavera, H., & Condori, C. (2014). Response of the mantle to flat slab evolution: Insights from local S splitting beneath Peru. *Geophysical Research Letters*, *41*, 3438–3446. https://doi.org/10.1002/2014GL059943

Eleogram, B. (2014). *The application of zircon (U-Th)/He thermochronology to determine the timing and slip rate on the Willard thrust, Sevier fold and thrust belt, Northern Utah*. (p. 140). Las Vegas: University of Nevada.

Engebretson, D. C., Cox, A., & Gordon, R. G. (1985). Relative motions between oceanic and continental plates in the Pacific basin. *Geological Society of America Special Papers*, *206*, 1–60. https://doi.org/10.1130/SPE206-p1

Erslev, E. A., Schmidt, C. J., Chase, R. B., & Erslev, E. A. (1993). Thrusts, back-thrusts, and detachment of Rocky Mountain foreland arches. In C. J. Schmidt, R. B. Chase & E. A. Erslev (Eds.), *Laramide basement deformation in the Rocky Mountain foreland of the western United States* (Vol. 280, pp. 339–358). Boulder, CO: Geological Society America. https://doi.org/10.1130/SPE280-p339

Espurt, N., Baby, P., Brusset, S., Roddaz, M., Hermoza, W., & Barbarand, J. (2010). The Nazca Ridge and uplift of the Fitzcarrald Arch: Implications for regional geology in northern South America. In C. Hoorn & F. P. Wesselingh (Eds.), *Amazonia: Landscape and Species Evolution* (pp. 89–100). Chichester: John Wiley & Sons Ltd. https://doi.org/10.1002/9781444306408.ch6

Fan, M., & Carrapa, B. (2014). Late Cretaceous–early Eocene Laramide uplift, exhumation, and basin subsidence in Wyoming: Crustal responses to flat slab subduction. *Tectonics*, *33*, 509–529. https://doi.org/10.1002/2012TC003221

Fan, M., DeCelles, P. G., Gehrels, G. E., Dettman, D. L., Quade, J., & Peyton, S. L. (2011). Sedimentology, detrital zircon geochronology, and stable isotope geochemistry of the lower Eocene strata in the Wind River basin, Central Wyoming. *GSA Bulletin*, *123*(5–6), 979–996. https://doi.org/10.1130/B30235.1

Fan, M., & Dettman, D. L. (2009). Late Paleocene high Laramide ranges in Northeast Wyoming: Oxygen isotope study of ancient river water. *Earth and Planetary Science Letters*, *286*(1–2), 110–121. https://doi.org/10.1016/j.epsl.2009.06.024

Fanti, F., & Catuneanu, O. (2010). Fluvial sequence stratigraphy: The wapiti formation, west-Central Alberta, Canada. *Journal of Sedimentary Research*, *80*(4), 320–338. https://doi.org/10.2110/jsr.2010.033

Feinstein, S., Kohn, B., Osadetz, K., Price, R. A., Sears, J. W., Harms, T. A., & Evenchick, C. A. (2007). Thermochronometric reconstruction of the prethrust paleogeothermal gradient and initial thickness of the Lewis thrust sheet, southeastern Canadian Cordillera foreland belt. In J. W. Sears, T. A. Harms & C. A. Evenchick (Eds.), *Whence the mountains? Inquiries into the evolution of orogenic systems: A volume in honor of Raymond A. Price* (Vol. 433, pp. 167–182). Boulder, CO: Geological Society of America. https://doi.org/10.1130/2007.2433(08)

Flament, N., Gurnis, M., Müller, R. D., Bower, D. J., & Husson, L. (2015). Influence of subduction history on South American topography. *Earth and Planetary Science Letters*, *430*, 9–18.

Foster-Baril, Z. S. (2017). *Eocene basin records of volcanism, topography, and tectonics in southern British Columbia, Canada* (p. 85), University of Idaho.

Fuentes, F., DeCelles, P. G., & Constenius, K. N. (2012). Regional structure and kinematic history of the Cordilleran fold-thrust belt in northwestern Montana, USA. *Geosphere*, GES00773. 00771.

Fulton, R., & Walcott, R. (1975). Lithospheric flexure as shown by deformation of glacial lake shorelines in southern British Columbia. In E. H. T. Whitten (Ed.), *Quantitative studies in the geological sciences*, *Memoir* (pp. 163–173). Boulder, CO: Geological Society of America.

Gao, M., & Fan, M. (2018). Depositional environment, sediment provenance and oxygen isotope paleoaltimetry of the early Paleogene greater Green River Basin, southwestern Wyoming, U.S.A. *American Journal of Science*, *318*(10), 1018–1055. https://doi.org/10.2475/10.2018.02

Gao, M., Fan, M., & Moucha, R. (2016). Southwestward weakening of Wyoming lithosphere during the Laramide orogeny. *Journal of Geophysical Research: Solid Earth*, *121*, 6219–6234. https://doi.org/10.1002/2016JB013130

Giallorenzo, M. A. (2013). *Application of (U-Th)/He and $^{40}Ar/^{39}Ar$ thermochronology to the age of thrust faulting in the Sevier orogenic belt*. (p. 297). Las Vegas: University of Nevada.

Göğüş, O. H., & Pysklywec, R. N. (2008). Near-surface diagnostics of dripping or delaminating lithosphere. *Journal of Geophysical Research*, *113*, B11404. https://doi.org/10.1029/2007JB005123

Gurnis, M. (1992). Rapid continental subsidence following the initiation and evolution of subduction. *Science*, *255*(5051), 1556–1558. https://doi.org/10.1126/science.255.5051.1556

Hardebol, N. J., Callot, J. P., Faure, J. L., Bertotti, G., & Roure, F. (2007). *Kinematics of the SE Canadian fold and thrust belt: Implications for the thermal and organic maturation history*. Berlin Heidelberg, Berlin, Heidelberg: Springer.

Harlan, S. S., Geissman, J. W., Whisner, S. C., & Schmidt, C. J. (2008). Paleomagnetism and geochronology of sills of the Doherty Mountain area, southwestern Montana: Implications for the timing of fold-and-thrust belt deformation and vertical-axis rotations along the southern margin of the Helena salient. *GSA Bulletin*, *120*(9–10), 1091–1104. https://doi.org/10.1130/b26313.1

Heller, P. L., Angevine, C. L., Winslow, N. S., & Paola, C. (1988). 2-phase stratigraphic model of foreland basin sequences. *Geology*, *16*(6), 501–504. https://doi.org/10.1130/0091-7613(1988)016<0501:TPSMOF>2.3.CO;2

Heller, P. L., & Liu, L. (2016). Dynamic topography and vertical motion of the U.S. Rocky Mountain region prior to and during the Laramide orogeny. *Geological Society of America Bulletin*, *128*(5–6), 973–988. https://doi.org/10.1130/b31431.1

Hetenyi, M. (1979). *Beams on elastic foundation* (p. 255). Ann Arbor: University of Michigan Press.

Hildebrand, R. S. (2014). Geology, mantle tomography, and inclination corrected Paleogeographic trajectories support westward subduction during Cretaceous orogenesis in the north American Cordillera. *Geoscience Canada*, *41*(2), 207–224. https://doi.org/10.12789/geocanj.2014.41.032

Humphreys, E. (2009). Relation of flat subduction to magmatism and deformation in the western United States. In S. M. Kay, V. A. Ramos & W. R. Dickinson (Eds.), *Backbone of the Americas: Shallow subduction, plateau uplift, and ridge and terrane collision* (Vol. 204, pp. 85–98). Boulder, CO: Geological Society of America.

Humphreys, E., Hessler, E., Dueker, K., Farmer, G. L., Erslev, E., & Atwater, T. (2003). How Laramide-age hydration of north American lithosphere by the Farallon slab controlled subsequent activity in the Western United States. *International Geology Review*, *45*(7), 575–595. https://doi.org/10.2747/0020-6814.45.7.575

Humphreys, E. D. (1995). Post-Laramide removal of the Farallon slab, western United States. *Geology*, *23*(11), 987–990. https://doi.org/10.1130/0091-7613(1995)023<0987:Plrotf>2.3.Co;2

Hyndman, R. D., Currie, C. A., Mazzotti, S., & Frederiksen, A. (2009). Temperature control of continental lithosphere elastic thickness, *Te* vs. *Earth and Planetary Science Letters*, *277*(3–4), 539–548. https://doi.org/10.1016/j.epsl.2008.11.023

Jadamec, M. A., Billen, M. I., & Roeske, S. M. (2013). Three-dimensional numerical models of flat slab subduction and the Denali fault driving deformation in south-Central Alaska. *Earth and Planetary Science Letters*, *376*, 29–42. https://doi.org/10.1016/j.epsl.2013.06.009

Johnson, R. C., Finn, T. M., & Roberts, S. B. (2004). Regional stratigraphic setting of the Maastrichtian rocks in the central Rocky Mountain region. In J. W. Robinson, & K. W. Shaley (Eds.), *Jonah Field: Case study of a giant tight-gas fluvial reservoir* (pp. 21–35). Oklahoma City: American Association of Petroleum Geologists.

Johnston, S. T. (2001). The great Alaskan Terrane wreck: Reconciliation of paleomagnetic and geological data in the Northern Cordillera. *Earth and Planetary Science Letters*, *193*(3-4), 259–272. https://doi.org/10.1016/S0012-821X(01)00516-7

Jones, C. H., Farmer, G. L., Sageman, B., & Zhong, S. (2011). Hydrodynamic mechanism for the Laramide orogeny. *Geosphere*, *7*(1), 183–201. https://doi.org/10.1130/ges00575.1

Jordan, T. E. (1981). Thrust loads and foreland basin evolution, cretaceous, western United States. *American Association of Petroleum Geologists Bulletin*, *65*(12), 2506–2520.

Jordan, T. E., Flemings, P. B., & Beer, J. A. (1988). Dating thrust-fault activity by use of foreland-basin strata. In K. L. Kleinspehn, & C. Paola (Eds.), *New perspectives in basin analysis* (pp. 307–330). New York, NY: Springer New York. https://doi.org/10.1007/978-1-4612-3788-4_16

Karlstrom, K. E., Coblentz, D., Dueker, K., Ouimet, W., Kirby, E., van Wijk, J., et al. (2012). Mantle-driven dynamic uplift of the Rocky Mountains and Colorado plateau and its surface response: Toward a unified hypothesis. *Lithosphere*, *4*(1), 3–22. https://doi.org/10.1130/l150.1

Karner, G. D., & Watts, A. B. (1983). Gravity anomalies and flexure of the lithosphere at mountain ranges. *Journal of Geophysical Research*, *88*(B12), 10,449–10,477. https://doi.org/10.1029/JB088iB12p10449

Kay, S. M., & Coira, B. L. (2009). Shallowing and steepening subduction zones, continental lithospheric loss, magmatism, and crustal fl ow under the central Andean Altiplano-Puna plateau. In S. M. Kay, V. A. Ramos, & W. R. Dickinson (Eds.), *Backbone of the Americas: Shallow subduction, plateau uplift, and ridge and terrane collision* (pp. 229–259). Boulder: Geological Society of America. https://doi.org/10.1130/2009.1204(11)

Kelley, S. A. (2005). Low-temperature cooling histories of the Cheyenne Belt and Laramie peak shear zone, Wyoming, and the Soda Creek-Fish Creek shear zone, Colorado. In K. E. Karlstrom & G. R. Keller (Eds.), *The Rocky Mountain Region: An Evolving Lithosphere*, *Geophysical Monograph* (Vol. 154, pp. 55–70). Washington, DC: American Geophysical Union. https://doi.org/10.1029/154gm05

Kelley, S. A., & Chapin, C. E. (1997). Internal structure of the southern front range, Colorado, from an apatite fissiontrack thermochronology perspective. In D. W. Bolyard, & S. A. Sonnenberg (Eds.), *Geologic history of the Colorado Front Range field trip guidebook* (pp. 19–30). Denver: Rocky Mountain Association of Geologists.

Kelley, S. A., & Chapin, C. E. (2004). Denudation history and internal structure of the front range and Wet Mountains, Colorado, based on apatite-fission-track thermochronology. *New Mexico Bureau of Geology and Mineral Resources Bulletin*, *160*, 41–68.

Kelley, S. A., Karlstrom, K. E., Stockli, D., McKeon, R., Hoffman, M., Lee, J., et al. (2010). A summary and evaluation of thermochronologic constraints on the exhumation history of the Colorado plateau–Rocky Mountain region, paper presented at CREvolution 2—Origin and evolution of the Colorado River system, workshop *Abstracts: US Geological Survey Open-File Report 2011-1210*.

Kendall, J., Vergés, J., Koshnaw, R., & Louterbach, M. (2019). Petroleum tectonic comparison of fold and thrust belts: The Zagros of Iraq and Iran, the Pyrenees of Spain, the Sevier of Western USA and the Beni Sub-Andean of Bolivia. *Geological Society, London, Special Publications*, *490*, SP490–2018-2102. https://doi.org/10.1144/sp490-2018-102

Kraig, D. H., Wiltschko, D. V., Spang, J. H., Schmidt, C., & Perry, W. (1988). The interaction of the Moxa arch (La barge platform) with the cordilleran thrust belt, south of Snider Basin, southwestern Wyoming. *Geological Society of America Memoirs*, *171*, 395–410. https://doi.org/10.1130/MEM171-p395

Krystopowicz, N. J., & Currie, C. A. (2013). Crustal eclogitization and lithosphere delamination in orogens. *Earth and Planetary Science Letters*, *361*, 195–207. https://doi.org/10.1016/j.epsl.2012.09.056

Landman, R. L., & Flowers, R. M. (2013). (U-Th)/He thermochronologic constraints on the evolution of the northern Rio Grande Rift, Gore Range, Colorado, and implications for rift propagation models. *Geosphere*, *9*(1), 170–187. https://doi.org/10.1130/ges00826.1

Larson, K. P., & Price, R. A. (2006). The southern termination of the Western Main ranges of the Canadian Rockies, near Fort Steele, British Columbia: Stratigraphy, structure, and tectonic implications. *Bulletin of Canadian Petroleum Geology*, *54*(1), 37–61. https://doi.org/10.2113/54.1.37

Lawton, T. F. (2008). Laramide sedimentary basins. In A. D. Miall (Ed.), *Sedimentary basins of the world* (pp. 429–450). Amsterdam: Elsevier. https://doi.org/10.1016/S1874-5997(08)00012-9

Leary, R., DeCelles, P., Gehrels, G., & Morriss, M. (2015). Fluvial deposition during transition from flexural to dynamic subsidence in the cordilleran foreland basin: Ericson formation, Western Wyoming, USA. *Basin Research*, *27*(4), 495–516. https://doi.org/10.1111/bre.12085

Lee, C. (2005). Trace element evidence for hydrous metasomatism at the base of the North American lithosphere and possible association with Laramide low-angle subduction. *The Journal of Geology*, *113*(6), 673–685. https://doi.org/10.1086/449327

Lee, C.-T., Yin, Q., Rudnick, R. L., & Jacobsen, S. B. (2001). Preservation of ancient and fertile lithospheric mantle beneath the southwestern United States. *Nature*, *411*(6833), 69–73. https://doi.org/10.1038/35075048

Lefebre, G. B. (1988). Tectonic evolution of Hanna Basin, Wyoming: Laramide block rotation in the Rocky Mountain foreland, Wyoming University, Laramie, WY (USA).

Li, Z. X. A., Lee, C. T. A., Peslier, A. H., Lenardic, A., & Mackwell, S. J. (2008). Water contents in mantle xenoliths from the Colorado plateau and vicinity: Implications for the mantle rheology and hydration-induced thinning of continental lithosphere. *Journal of Geophysical Research*, *113*, B09210. https://doi.org/10.1029/2007JB005540

Liu, L., & Gurnis, M. (2010). Dynamic subsidence and uplift of the Colorado plateau. *Geology*, *38*(7), 663–666. https://doi.org/10.1130/G30624.1

Liu, L., Gurnis, M., Seton, M., Saleeby, J., Muller, R. D., & Jackson, J. M. (2010). The role of oceanic plateau subduction in the Laramide orogeny. *Nature Geoscience*, *3*(5), 353–357. https://doi.org/10.1038/ngeo829

Liu, S., & Currie, C. A. (2016). Farallon plate dynamics prior to the Laramide orogeny: Numerical models of flat subduction. *Tectonophysics*, *666*(Supplement C), 33–47. https://doi.org/10.1016/j.tecto.2015.10.010

Liu, S., & Nummedal, D. (2004). Late Cretaceous subsidence in Wyoming: Quantifying the dynamic component. *Geology*, *32*(5), 397–400. https://doi.org/10.1130/g20318.1

Liu, S., Nummedal, D., & Gurnis, M. (2014). Dynamic versus flexural controls of Late Cretaceous Western Interior Basin, USA. *Earth and Planetary Science Letters*, *389*, 221–229. https://doi.org/10.1016/j.epsl.2014.01.006

Livaccari, R. F., Burke, K., & Şengör, A. M. C. (1981). Was the Laramide orogeny related to subduction of an oceanic plateau? *Nature*, *289*(5795), 276–278. https://doi.org/10.1038/289276a0

Livaccari, R. F., & Perry, F. V. (1993). Isotopic evidence for preservation of cordilleran lithospheric mantle during the Sevier-Laramide orogeny, western United States. *Geology*, *21*(8), 719–722. https://doi.org/10.1130/0091-7613(1993)021<0719:IEFPOC>2.3.CO;2

Lowry, A. R., & Smith, R. B. (1994). Flexural rigidity of the Basin and Range-Colorado Plateau-Rocky Mountain transition from coherence analysis of gravity and topography. *Journal of Geophysical Research*, *99*(B10), 20,123–20,140. https://doi.org/10.1029/94JB00960

Lowry, A. R., & Smith, R. B. (1995). Strength and rheology of the western US Cordillera. *Journal of Geophysical Research*, *100*(B9), 17,947–17,963. https://doi.org/10.1029/95JB00747

Lynds, R. M., & Lichtner, D. T. (2016). Stratigraphy and hydrocarbon potential of the fort union and lance formations in the Great Divide and Washakie basins, South-Central Wyoming, *Wyoming State Geological Survey Report of Investigations*, 73, 70.

Lyon-Caen, H., & Molnar, P. (1983). Constraints on the structure of the Himalaya from an analysis of gravity-anomalies and a flexural model of the lithosphere. *Journal of Geophysical Research*, *88*(NB10), 8171–8191. https://doi.org/10.1029/JB088iB10p08171

Matson, R. M., & Magathan, W. J. (2017). Hanna of Wyoming—The Rockies' Deepest Basin. *The Mountain Geologist*, *54*(4), 265–293. https://doi.org/10.31582/rmag.mg.54.4.265

McKenzie, D., & Fairhead, D. (1997). Estimates of the effective elastic thickness of the continental lithosphere from Bouguer and free air gravity anomalies. *Journal of Geophysical Research*, *102*(B12), 27,523–27,552. https://doi.org/10.1029/97JB02481

Mitrovica, J. X., Beaumont, C., & Jarvis, G. T. (1989). Tilting of continental interiors by the dynamical effects of subduction. *Tectonics*, *8*(5), 1079–1094. https://doi.org/10.1029/TC008i005p01079

Mix, H. T., Mulch, A., Kent-Corson, M. L., & Chamberlain, C. P. (2011). Cenozoic migration of topography in the North American Cordillera. *Geology*, *39*(1), 87–90. https://doi.org/10.1130/g31450.1

Moucha, R., Forte, A. M., Rowley, D. B., Mitrovica, J. X., Simmons, N. A., & Grand, S. P. (2008). Mantle convection and the recent evolution of the Colorado plateau and the Rio Grande Rift valley. *Geology*, *36*(6), 439–442. https://doi.org/10.1130/G24577A.1

Mulch, A., Teyssier, C., Cosca, M. A., & Chamberlain, C. P. (2007). Stable isotope paleoaltimetry of Eocene core complexes in the North American Cordillera. *Tectonics*, *26*, TC4001. https://doi.org/10.1029/2006TC001995

Naeser, C., Bryant, B., Kunk, M., Kellogg, K., Donelick, R., Perry, W., et al. (2002). Tertiary cooling and tectonic history of the White River uplift, Gore range, and western Front range, Central Colorado: Evidence from fission-track and $^{39}Ar/^{40}Ar$ ages, Late Cenozoic evaporite tectonism and volcanism in west-central Colorado. *Geological Society of America Special Paper*, *366*, 31–54.

Nelson, J. L., Colpron, M., & Israel, S. (2013). The Cordillera of British Columbia, Yukon, and Alaska: Tectonics and metallogeny. In M. Colpron T. Bissig B. G. Rusk & J. F. H. Thompson (Eds.), *Tectonics, metallogeny, and discovery: The North American Cordillera and similar accretionary settings* (Vol. 17, pp. 53–110). Littleton, CO: Society of Economic Geologists. https://doi.org/10.5382/sp.17.03

Omar, G. I., Lutz, T. M., & Giegengack, R. (1994). Apatite fission-track evidence for Laramide and post-Laramide uplift and anomalous thermal regime at the Beartooth overthrust, Montana-Wyoming. *Geological Society of America Bulletin*, *106*(1), 74–85. https://doi.org/10.1130/0016-7606(1994)106<0074:AFTEFL>2.3.CO;2

Painter, C. S., & Carrapa, B. (2013). Flexural versus dynamic processes of subsidence in the north American cordillera foreland basin. *Geophysical Research Letters*, *40*, 4249–4253. https://doi.org/10.1002/grl.50831

Pană, D. I., & van der Pluijm, B. A. (2015). Orogenic pulses in the Alberta Rocky Mountains: Radiometric dating of major faults and comparison with the regional tectono-stratigraphic record. *GSA Bulletin*, *127*(3–4), 480–502. https://doi.org/10.1130/b31069.1

Peyton, S. L., & Carrapa, B. (2013). An overview of low-temperature thermochronology in the Rocky Mountain and its application to petroleum system analysis. In C. Knight, & J. Cuzella (Eds.), *Application of structural methods to Rocky Mountain hydrocarbon exploration and development* (pp. 37–70). Tulsa: AAPG Studies in Geology.

Peyton, S. L., Reiners, P. W., Carrapa, B., & DeCelles, P. G. (2012). Low-temperature thermochronology of the northern Rocky Mountains, western USA. *American Journal of Science*, *312*(2), 145–212. https://doi.org/10.2475/02.2012.04

Price, R. (1994). Cordilleran tectonics and the evolution of the Western Canada sedimentary basin. In G. D. Mossop, & I. Shetsen (Eds.), *Geological Atlas of Western Canada* (pp. 13–24). Calgary: Canadian Society of Petroleum Geologistse-Alberta Research Council.

Price, R., & Mountjoy, E. (1970). Geologic structure of the Canadian Rocky Mountains between bow and Athabasca Rivers: A progress report. *Geological Association of Canada Special Paper*, *6*, 7–25.

Quinlan, G. M., & Beaumont, C. (1984). Appalachian thrusting, lithospheric flexure, and the Paleozoic stratigraphy of the eastern interior of North America. *Canadian Journal of Earth Sciences*, *21*(9), 973–996. https://doi.org/10.1139/e84-103

Raynolds, R. G. (2002). Upper Cretaceous and Tertiary stratigraphy of the Denver Basin, Colorado, Rocky Mt. *Geology*, *37*(2), 111–134. https://doi.org/10.2113/gsrocky.37.2.111

Robinson-Roberts, L. N., & Kirschbaum, M. A. (1995). *Paleogeography of the Late Cretaceous of the Western interior of middle North America; coal distribution and sediment Accumulation* (pp. 120). Denver, CO: USGS.

Roehler, H. W. (1965). Summary of pre-Laramide Late Cretaceous sedimentation in the Rock Springs uplift area. In R. H. Devoto, & R. K. Bitter (Eds.), *Sedimentation of Late Cretaceous and Tertiary outcrops, Rock Springs uplift: Wyoming Geological Association 19th Field Conference Guidebook* (pp. 10–12). Casper, WY: Wyoming Geological Association.

Royden, L. H. (1993). The tectonic expression slab pull at continental convergent boundaries. *Tectonics*, *12*, 305–325.

Rudolph, K. W., Devlin, W. J., & Carabaugh, J. P. (2015). Upper Cretaceous sequence stratigraphy of the Rock Springs uplift, Wyoming. *The Mountain Geologist*, *52*(3), 13–157.

Saleeby, J. (2003). Segmentation of the Laramide slab—Evidence from the southern Sierra Nevada region. *Geological Society of America Bulletin*, *115*(6), 655–668. https://doi.org/10.1130/0016-7606(2003)115<0655:sotlsf>2.0.co;2

Saleeby, J., Farley, K. A., Kistler, R. W., & Fleck, R. J. (2007). Thermal evolution and exhumation of deep-level batholithic exposures, southernmost Sierra Nevada, California, *Geological Society of America Special Papers*, *419*, 39–66, doi:https://doi.org/10.1130/2007.2419(02)

Saylor, J. E., Jordan, J. C., Sundell, K. E., Wang, X., Wang, S., & Deng, T. (2017). Topographic growth of the Jishi Shan and its impact on basin and hydrology evolution, NE Tibetan Plateau. *Basin Research*, *30*(3), 544–563. https://doi.org/10.1111/bre.12264

Schmidt, M. W., & Poli, S. (2003). Generation of mobile components during subduction of oceanic crust. *Treatise on Geochemistry*, *3*, 659.

Schwartz, R. K., & DeCelles, P. G. (1988). Cordilleran foreland basin evolution in response to interactive Cretaceous thrusting and foreland partitioning, Southwestern Montana. In C. J. Schmidt, & J. W. J. Perry (Eds.), *Interaction of the Rocky Mountain foreland and the Cordilleran thrust belt* (Vol. 71, pp. 489–513). Boulder, CO: Geological Society of America.

Sheffels, B., & McNutt, M. (1986). Role of subsurface loads and regional compensation in the isostatic balance of the transverse ranges, California: Evidence for intracontinental subduction. *Journal of Geophysical Research*, *91*(B6), 6419–6431. https://doi.org/10.1029/JB091iB06p06419

Shuster, M. W., & Steidtmann, J. R. (1988). Tectonic and sedimentary evolution of the northern Green River basin, western Wyoming. In C. J. Schmidt, & J. W. J. Perry (Eds.), *Interaction of the Rocky Mountain foreland and the Cordilleran thrust belt* (Vol. 171, pp. 515–529). Boulder, CO: Geological Society of America.

Sigloch, K., McQuarrie, N., & Nolet, G. (2008). Two-stage subduction history under North America inferred from multiple-frequency tomography. *Nature Geoscience*, *1*(7), 458–462. https://doi.org/10.1038/ngeo231

Simony, P. S., & Carr, S. D. (2011). Cretaceous to Eocene evolution of the southeastern Canadian cordillera: Continuity of Rocky Mountain thrust systems with zones of "in-sequence" mid-crustal flow. *Journal of Structural Geology*, *33*(9), 1417–1434. https://doi.org/10.1016/j.jsg.2011.06.001

Sinclair, H. D., Coakley, B. J., Allen, P. A., & Watts, A. B. (1991). Simulation of Foreland Basin stratigraphy using a diffusion model of mountain belt uplift and erosion: An example from the Central Alps, Switzerland. *Tectonics*, *10*(3), 599–620. https://doi.org/10.1029/90TC02507

Smith, M. E., Carroll, A. R., & Singer, B. S. (2008). Synoptic reconstruction of a major ancient lake system: Eocene Green River formation, western United States. *Geological Society of America Bulletin*, *120*(1–2), 54–84. https://doi.org/10.1130/1326073.1

Smith, R. Y., Basinger, J. F., & Greenwood, D. R. (2009). Depositional setting, fossil flora, and paleoenvironment of the early Eocene Falkland site, Okanagan highlands, British Columbia. *Canadian Journal of Earth Sciences*, *46*(11), 811–822. https://doi.org/10.1139/E09-053

Snell, K. E., Koch, P. L., Druschke, P., Foreman, B. Z., & Eiler, J. M. (2014). High elevation of the 'Nevadaplano' during the Late Cretaceous. *Earth and Planetary Science Letters*, *386*, 52–63. https://doi.org/10.1016/j.epsl.2013.10.046

Sommer, H., & Gauert, C. (2011). Hydrating laterally extensive regions of continental lithosphere by flat subduction: A pilot study from the north American cordillera. *Journal of Geodynamics*, *51*(1), 17–24. https://doi.org/10.1016/j.jog.2010.05.006

Stevens, A. L., Balgord, E. A., & Carrapa, B. (2016). Revised exhumation history of the Wind River range, WY, and implications for Laramide tectonics. *Tectonics*, *35*, 1121–1136. https://doi.org/10.1002/2016TC004126

Stone, D. S. (2002). Morphology of the Casper Mountain uplift and related, subsidiary structures, Central Wyoming: Implications for Laramide kinematics, dynamics, and crustal inheritance. *AAPG Bulletin*, *86*(8), 1417–1440. https://doi.org/10.1306/61eedcba-173e-11d7-8645000102c1865d

Strickland, E. D., Singleton, J. S., & Haxel, G. B. (2018). Orocopia schist in the northern Plomosa Mountains, west-Central Arizona: A Laramide subduction complex exhumed in a Miocene metamorphic core complex. *Lithosphere*, *10*(6), 723–742. https://doi.org/10.1130/l742.1

Tesauro, M., Kaban, M. K., & Mooney, W. D. (2015). Variations of the lithospheric strength and elastic thickness in North America. *Geochemistry, Geophysics, Geosystems*, *16*, 2197–2220. https://doi.org/10.1002/2015GC005937

Tesauro, M., Kaban, M. K., Mooney, W. D., & Cloetingh, S. A. P. L. (2014). Density, temperature, and composition of the North American lithosphere—New insights from a joint analysis of seismic, gravity, and mineral physics data: 2. Thermal and compositional model of the upper mantle. *Geochemistry, Geophysics, Geosystems*, *15*, 4808–4830. https://doi.org/10.1002/2014GC005484

Tindall, S. E., Storm, L. P., Jenesky, T. A., & Simpson, E. L. (2010). Growth faults in the Kaiparowits Basin, Utah, pinpoint initial Laramide deformation in the western Colorado plateau. *Lithosphere*, *2*(4), 221–231. https://doi.org/10.1130/L79.1

Torsvik, T. H., Müller, R. D., Van der Voo, R., Steinberger, B., & Gaina, C. (2008). Global plate motion frames: Toward a unified model. *Reviews of Geophysics*, *46*, RG3004. https://doi.org/10.1029/2007RG000227

Turcotte, D. L., & Schubert, G. (1982). *Geodynamics* (p. 848). Cambridge: Cambridge University Press.

Van Der Lee, S., & Frederiksen, A. (2005). Surface wave tomography applied to the North American upper mantle. *Seismic Earth: Array analysis of broadband seismograms*, *157*, 67–80.

van der Pluijm, B. A., Vrolijk, P. J., Pevear, D. R., Hall, C. M., & Solum, J. (2006). Fault dating in the Canadian Rocky Mountains: Evidence for Late Cretaceous and early Eocene orogenic pulses. *Geology*, *34*(10), 837–840. https://doi.org/10.1130/g22610.1

Walcott, R. I. (1970). Flexural rigidity, thickness, and viscosity of the lithosphere. *Journal of Geophysical Research*, *75*(20), 3941–3954. https://doi.org/10.1029/JB075i020p03941

Wangen, M. (2010). *Physical principles of sedimentary basin analysis* (p. 527). Cambridge: Cambridge University Press. https://doi.org/10.1017/CBO9780511711824

Watts, A. B. (2001). *Isostasy and flexure of the lithosphere* (p. 458). Cambridge: Cambridge University Press.

Watts, A. B., & Burov, E. B. (2003). Lithospheric strength and its relationship to the elastic and seismogenic layer thickness. *Earth and Planetary Science Letters*, *213*(1–2), 113–131. https://doi.org/10.1016/s0012-821x(03)00289-9

Whitmeyer, S. J., & Karlstrom, K. E. (2007). Tectonic model for the Proterozoic growth of North America. *Geosphere*, *3*(4), 220–259. https://doi.org/10.1130/ges00055.1

Yonkee, W., Parry, W., Bruhn, R., & Cashman, P. (1989). Thermal models of thrust faulting: Constraints from fluid-inclusion observations, Willard thrust sheet, Idaho-Utah-Wyoming thrust belt. *Geological Society of America Bulletin*, *101*(2), 304–313. https://doi.org/10.1130/0016-7606(1989)101<0304:TMOTFC>2.3.CO;2

Yonkee, W. A. (1992). Basement-cover relations, Sevier orogenic belt, northern Utah. *Geological Society of America Bulletin*, *104*(3), 280–302. https://doi.org/10.1130/0016-7606(1992)104<0280:bcrsob>2.3.co;2

Yonkee, W. A., Eleogram, B., Wells, M. L., Stockli, D. F., Kelley, S., & Barber, D. E. (2019). Fault slip and exhumation history of the Willard thrust sheet, Sevier fold-Thrust Belt, Utah: Relations to wedge propagation, hinterland uplift, and Foreland Basin sedimentation. *Tectonics*, *38*, 2850–2893. https://doi.org/10.1029/2018TC005444

Yonkee, W. A., & Weil, A. B. (2015). Tectonic evolution of the Sevier and Laramide belts within the north American Cordillera orogenic system. *Earth-Science Reviews*, *150*, 531–593. https://doi.org/10.1016/j.earscirev.2015.08.001

Zandt, G., Leidig, M., Chmielowski, J., Baumont, D., & Yuan, X. (2003). Seismic detection and characterization of the Altiplano-Puna magma body, Central Andes. *Pure and Applied Geophysics*, *160*(3), 789–807. https://doi.org/10.1007/PL00012557